The Śnieżka peatland as a candidate for the Global Boundary Stratotype Section and Point for the Anthropocene Series

Barbara Fialkiewicz-Koziel, Edyta Łokas, Beata Smieja-Król, Simon Turner, Francois de Vleeschouwer, Michal Woszczyk, Katarzyna Marcisz, Mariusz Galka, Mariusz Lamentowicz, Piotr Kolaczek, et al.

The Śnieżka peatland

as a candidate for the Global Boundary Stratotype Section and Point for the

Anthropocene Series

Fiałkiewicz-Kozieł B.[1], Łokas E.[2], Smieja-Król B.[3], Turner S.D.[4],

De Vleeschouwer F.[5], Woszczyk M.[1], Marcisz K.[6], Gałka M.[7], Lamentowicz M.[6],

Kołaczek P.[6], Hajdas I.[8], Karpińska-Kołaczek M.[6], Kołtonik K.[2], Mróz T.[9], Roberts

S.L.[4], Rose N.L.[4], Krzykawski T.[3],Boom A.[10], Yang H.[4]

1. Adam Mickiewicz University, Institute of Geoecology and Geoinformation, Krygowskiego 10, Poznań, Poland.
2. Institute of Nuclear Physics, Polish Academy of Sciences, Radzikowskiego 152, 31-342 Kraków, Poland.
3. University of Silesia, Institute of Earth Sciences, Faculty of Natural Sciences, Będzińska 60, 41-200 Sosnowiec, Poland.
4. Environmental Change Research Centre, Department of Geography, University College London, Gower Street, London WC1E 6BT. UK.
5. Instituto Franco-Argentino para el Estudio del Clima y sus Impactos (IRL IFAECI/CNRS-CONICET-UBA-IRD) Dpto. de Ciencias de la Atmosfera y los Oceanos, FCEN, Universidad de Buenos Aires Intendente Guiraldes 2160 - Ciudad Universitaria Pabellon II - 2do. Piso (C1428EGA) Ciudad Autonoma de Buenos Aires - Argentina
6. Climate Change Ecology Research Unit, Adam Mickiewicz University, Poznań, B. Krygowskiego 10, 61-680 Poznań, Poland
7. University of Lodz, Faculty of Biology and Environmental Protection, Department of Geobotany and Plant Ecology, Banacha 12/16, Lodz, Poland.
8. Laboratory of Ion Beam Physics, ETH Zurich, Zurich, Switzerland
9. Institute of Physics, Jagiellonian University, Kraków, 30-348, Poland
10. School of Geography, Geology and the Environment, University of Leicester,University Road,Leicester, LE1 7RH, UK.

Abstract

The subalpine, atmospherically fed Śnieżka peatland, located in the Polish part of the Sudetes, is one of the nominated candidates for the GSSP of the Anthropocene. Data from two profiles, Sn1 (2012) and Sn0 (2020), from this site are critical for distinguishing the proposed epoch, while an additional core Sn2 is presented to support main evidence. The Sn0 archive contains a wide array of critical markers such as plutonium (Pu), radiocarbon ($F^{14}C$), fly ash particles, Hg and stable C and N isotopes which are consistent with the previously well documented $^{210}Pb/^{14}C$ dated Sn1 profile, which provides a high-resolution and comprehensive database of trace elements and rare earth elements (REE), Pb isotopes, Pu, Cs, pollen, and testate amoebae.

The 1952 worldwide appearance of Pu, owing to its global synchronicity and repeatability between the cores, is proposed here as a primary marker of the Anthropocene, supported by the prominent upturn of selected chemostratigraphic and biostratigraphic indicators as well as the appearance of technofossils and artificial radionuclides.

Key words: The Sudetes, Stratotype of Anthropocene, Plutonium, Great Acceleration, Trace elements, Testate Amoebae, SCP, SAP, *Ambrosia artemissifolia*

1. Introduction Peatlands cover around 2-3% of the Earth continental surface (Xu et al., 2018) and, owing to sequestration/release of CO_2, play a crucial role in the regulation of global climate (Yu, 2012; Loisel et al., 2014; Gallego-Salla et al., 2018). At the same time, peatlands are excellent repositories of past and recent environmental changes (Shotyk, 1998; De Vleeschower et al., 2010a). The stability of peatlands and their ability to accumulate carbon (C) is affected by climate, in particular air temperature and precipitation, atmospheric pollution, fire, sea level, permafrost thawing, and land use (Loisel et al., 2021). Even though these factors operate on different temporal and spatial scales, the peatlands vulnerability to environmental change varies geographically (Turetsky et al., 2014). Millar et al. (2017) claimed that subalpine mires were more stable C reservoirs compared to lowland peatlands, and consequently, they provide highly reliable records of environmental changes (Rangwala and Miller, 2012), as confirmed by many studies (e.g., Bao et al., 2015; Hansson et al., 2017; Fiałkiewicz-Kozieł et al., 2022). The Sudetes are a central European mountain range located between Poland and the Czech Republic, within the so-called Black Triangle, one of the most polluted areas of Europe (Fig. 1). The subalpine Śnieżka peatland within the highest Karkonosze mountain range of the Sudetes provides an excellent opportunity to gain an insight into the long-ranged dispersal of transboundary traces of human activity and thus to investigate the negative human impact on the environment within the recent past.

Evidence of human activity in the Sudetes extends back to Paleolithic settlements and later Neolithic agriculture (Valde-Nowak, 1999). From the 3rd century BCE, there is evidence of the exploitation of river-deposited gold by Celts (Woźniak, 1970). The intense mining of rich metal ores (gold and precious minerals) in the region commenced in the 12th century (Julkowska, 2016). By the 20th century, numerous mines, factories, and power plants made the region one of the most polluted in Europe (Grübler, 2002; Kolar et al., 2015). In the 1970s, the synergistic impact of extremely high levels of acid rain, alkali ashes, and insect outbreaks caused significant damage to coniferous forests in this area and directly affected human health (Mazurski, 1986). The signing of a joint declaration on cooperation in solving environmental problems in the Black Triangle by the German, former Czechoslovakian, and Polish governments in 1991 prompted the improvement and protection of the area (Grübler, 2002; Kolar et al., 2015).

The unprecedented pollution level in the Sudetes region created a need for scientific assessment of the quality of the environment. The most severely affected Izery Mts range (Zuna et al., 2011; Glina, Bogacz, 2013; Magiera et al., 2019) received major attention. Since the time the problem was identified, many reports on acid rain (Mazurski 1986), dust mineralogy, pollen analysis, sulphur and carbon isotopes (i.e., Speranza et al., 2000; Popowski, 2005; Skrzypek et al., 2009; Kajukało et al., 2016), magnetic susceptibility and geochemistry (i.e., Strzyszcz and Magiera, 2001; Fiałkiewicz-Kozieł et al., 2015;

Bińczycki et al., 2020), ecology and anthropopressure (Wojtuń et al., 2018; Pech et al., 2022) have been published.

However, the Śnieżka peatland (Sn) has the most comprehensive, high-resolution geochemical and palaeoecological record in the Sudetes. Concentrations of Pb, Zn, Cu, Ni, Cr, Ti, Al, U, Sc, rare earth elements (REE), mineralogy, and ^{204}Pb, ^{206}Pb, ^{207}Pb, ^{208}Pb, ^{234}U, ^{137}Cs, $^{239+240}$Pu have been determined (Fiałkiewicz-Kozieł et al., 2020). This study revealed the presence of both regional and global trends in the stratigraphic record, such as the combustion of fossil fuels, the catastrophic release of artificial radionuclides during the Chernobyl accident, and atmospheric nuclear weapon tests. The quality of the record was the basis for nominating the Śnieżka Peatland as a GSSP candidate for the Anthropocene series (AWG, 2020; Luciano, 2022).

The preparatory activities of the Anthropocene Working Group, including events leading to the submission of GSSP proposals and the binding decision that the base of the Anthropocene should align with stratigraphic signals dating to the mid-20th century, are detailed in the introductory article to this special issue (Waters et al., 2022).

This paper aims to review the geochemical and paleoecological data from the Śnieżka candidate site. The data presented involves three cores (Sn0, Sn1, and Sn2). Special focus is placed on the Sn0 core (2020), which provides the most representative continuous record containing the possible GSSP. This is supported by additional detailed

data from Sn1 (2012), and the summary is based on both profiles. Data from Sn2 (2012) are also presented to support these results.

2. Materials and methods

2.1 Geographic setting The study site is located in the Polish part of the Sudetes mountains. The Śnieżka peatland (50°44′N, 15°42'E) is developed on a plateau (1440 m a.s.l.) in the Karkonosze range, close to the highest summit of Mt. Śnieżka (1602 m a.s.l.; Fig. 1).

The mountain range is a significant orographic barrier for regional-continental air masses, and the dominated winds are westerlies (Sobik et al., 2014). For 64% of the year, the area is directly influenced by the zonal circulation of oceanic air masses from the North Atlantic, flowing over the lowlands of Western Europe. Thirty percent of the year is characterised by polar continental air masses flowing from the east, 4% by arctic air from the north, and 2% by tropical air masses from the south (Sobik et al., 2014). The mean annual air temperature at Mt. Śnieżka, based on 1881-2012 measurements, is +0.5 °C. The lowest annual mean temperature of –1.2 °C was observed in 1941, and the highest value of +2.3 °C was registered in 2000, 2006, and 2011 (Urban and Tomczyński, 2017). The annual precipitation is ∼1500 mm (Sobik et al., 2014; Migała et al., 2016). The present plant community of the peatland consists of *Sphagnum lindbergii, Sphagnum balticum, Carex limosa, Carex rostrata, Baeothryon caespitosum, Eriophorum*

vaginatum, *Carex limosa*, *Carex rostrata*, *Empetrum hermaphroditum*, *Andromeda polifolia*, *Oxycoccus palustris*, and *Rubus chamaemorus* as well as dwarf *Pinus mugo* (Wojtuń, 2006).

2.2 Sampling

Cores Sn1 and Sn2 (63 and 67 cm in length, respectively) were retrieved in the spring of 2012, and 50 cm long GSSP core - Sn0 was collected in the summer of 2020 using a stainless-steel 10×10×100 cm Wardenaar corer (Wardenaar, 1987). The distance between all three cores is approximately 15m (Sn0: 50°44′20,90″N, 15°42′28,03″E; Sn1: 50°44′21,40″N, 15°42′28,23″E', Sn2: 50°44′20,67″N, 15°42′29,44″E). The monoliths were sealed in plastic bags, transported to the laboratory in Poznań (Adam Mickiewicz University - AMU), and stored in the laboratory fridge. Cores were cut into 1-cm thick slices (except the top 6 cm of Sn1 and Sn2, which were cut in 2-cm slices) using a carbon steel knife.

While Sn1 and Sn2 preparation followed the procedure described in Givelet et al. (2004) and De Vleeschouwer et al. (2010b), Sn0 was only partially subsampled, and a complete 5cm x 5cm x 50cm core is retained as an archive in a cold room (4ºC).

2.3 Methods A concise summary of the applied methods is provided below. A detailed description of all methods can be found in Suppl.1 and Fiałkiewicz et al. (2020) for Sn1

and Sn2. Physical properties and macrofossils were determined in every slice using standard methods (Givelet et al., 2004; De Vleeschouwer et al. 2010b). Activities of ^{210}Pb and ^{137}Cs were determined for each sub-sample of Sn0 by gamma-ray spectrometry using a high purity germanium detector (DSG, Germany) located at the Institute of Physics Jagiellonian University. Measurements of $^{238,\ 239+240}$Pu activities were undertaken using an alpha-particle spectrometer (Alpa Analyst, Canberra) with semiconductor, passivated planar silicon detectors (PIPS, Canberra). Fourteen samples of macrofossils from core Sn0 were analyzed at the AMS facility ETH Zurich. After the Acid-Base-Acid treatment (Hajdas 2008), samples were graphitized (Nemec et al., 2010) and analyzed using the MICADAS system (Synal et al., 2007). Total concentrations of elements (Sn1, Sn2) were measured using ICP-MS at the UAM for trace metals and Observatoire Midi-Pyrénées (Toulouse, France) for Rare Earth Elements. Mercury (Hg) (Sn0) was measured using cold vapour-atomic fluorescence spectrometry (CV-AFS). The measurements of stable lead (Pb) isotopes (Sn1, Sn2) were conducted on TIMS Finnigan MAT-261 special (UAM). Total nitrogen (N), carbon (C), and sulphur (S) values (Sn2) were determined in dried and homogenized samples with a VarioMax CNS elemental analyzer (Elementar Analyzensysteme GmbH, Germany). CN, C, and N isotopes (Sn0) were analysed on an elemental analyser (ANCA GSL, Sercon, UK). SCPs (Sn0) were determined using light microscopy following the procedure of Rose (1994). Dust particles were determined (all three profiles) using the backscattered electron detector (BSE) of a scanning electron

microscope (SEM) equipped with an energy-dispersive X-ray analysing system (SEM-FEI Quanta 250; University of Silesia in Katowice). Mullite content was determined in the profiles using x-ray diffraction (XRD), following the method described in Smieja-Król et al. (2019). Pollen and testate amoebae (Sn1) were determined using light microscopy following standard procedures. Non-metric multidimensional scaling (NMDS) was used to define the relationships between geochemical data, water table reconstruction, and the response of testate amoeba and vegetation (pollen data) to anthropogenic forcing.

3. Results

3.1 Physical properties and macrofossils The three investigated cores showed similar patterns of peat accumulation (Fig. 2). Initially, the peat layers were mainly composed of minerotrophic mosses such as *Sphagnum russowii* and *Straminergon stramineum*, then followed by *Sphagnum lindbergii* in cores Sn1 and Sn2. In the upper part of the three peat monoliths, *Polytrichum strictum* also played a meaningful role as a peat-forming species. In the topmost part of Sn2 *S. medium/divinum* and *S. balticum* re-appeared, indicating a more oligotrophic habitat. Importantly, the preferred boundary of the proposed Anthropocene series is not encompassed by the boundary of local macrofossil zones. The detailed description of macrofossils can be found in the supplementary material (Suppl.2).

The ash content (AC) in Sn0 and Sn1 is low (up to 6%) and shows more complex patterns compared to the botanical layering of peat. The Sn0 core has 2 zones with a boundary at c.a. 18 cm depth (Fig. 2). The lower zone has 2-4 % higher ash content values than the upper one. In Sn1, there is a slight enrichment in AC between 36 and 22 cm. In this layer, AC is between 2 and 5% compared to <2% in underlying and overlying peat.

In Sn2, AC distribution shows considerable variability especially below 17.5 cm depth, where there are three positive excursions of AC at ca. 42.5, 32.5, and 28 cm. Above 17.5 cm two layers can be identified with enhanced (up to 6%) AC values between 17 and 10 cm and <3% contents in the topmost 10 cm.

Higher and more numerous maxima of AC in Sn2 indicated possible disturbance. Therefore, we used Sn2 only to show some critical results, such as mullite and SAP appearance, which correspond to the proposed Anthropocene series level within the geochemical profile (Fig.4).

3.2 Radioisotopes (Sn0; Sn1) Activity concentrations of ^{137}Cs in both profiles (Sn0, Sn1) were comparable and ranged between 56 ± 2 Bqkg^{-1} to 2576 ± 55 Bqkg^{-1} (Fig.3). Most of the total Cs activity concentration in Sn1 is retained in the upper 9 cm-thick layer. Two distinct peaks of ^{137}Cs activity can be found at 23.5 cm (1011 ± 48 Bqkg^{-1}) and 26.5 cm depth (699 ± 58 Bqkg^{-1}). These peaks act as lithochronohorizons for the Chernobyl accident (1986) and the atmospheric nuclear weapon tests (1963), respectively.

In the Sn0 profile, three characteristic maxima of ^{137}Cs were observed. The uppermost was located just below the peat surface, albeit lower than in the Sn1. The second activity peak occurred between 18 and 20 cm (maximum at 17.5 cm) and can be related to the Chernobyl event (1986). The lowest Cs peak, at 27 - 29 cm, was assigned to the nuclear weapon tests (1963), which was corroborated by the nearby position of Pu maximum at 30.5 cm depth.

The first traces of $^{239+240}Pu$ occur at 45.5–46.5 cm depth in Sn1, with the maximum at 32.5-33.5 cm (Fig.3). The first distinct increase is recorded at a depth of 43.5–44.5 cm (Sn0), followed by a prominent peak at 30–31 cm depth, which correlates with the 1963 nuclear weapon tests. Above, the activity decreased continuously up-core until the next tiny peak recorded at 17–18 cm depth (Sn0) and 22.5-23.5 cm depth (Sn1), which correlates with the Chernobyl accident in 1986. The $^{239+240}Pu$ activities then declined to minimum detectable activity (MDC) and varied between 0.04 to 0.09 $Bqkg^{-1}$ in the upper part of the profiles Sn1 and Sn0.

Results of ^{14}C in Sn0 samples are expressed as $F^{14}C$ (fraction modern ^{14}C) (Reimer et al., 2004) and calibrated using the Bayesian sequence model of the OxCal calibration program (Ramsey, 2009) with the bomb peak atmospheric data for the Northern Hemisphere (Hua et al., 2021). Except for one sample (Sn0 37.5cm), all the samples follow the atmospheric NH bomb peak data (Supplementary Table 2; Fig. 10). The high value of $F^{14}C$ measured for sample Sn0 37.5 might be due to the intrusion of young

material into the lower layers of sediment. Consequently, the sample was not included in the OxCal model.

^{14}C modelling for Sn1 revealed 220 years of peat accumulation. The data obtained from ^{14}C activity suggests a hiatus in the Sn2 profile. Therefore, for further interpretation, only the top 44 cm, which spans a similar time interval compared to Sn1, were used for interpretation.

3.3 ^{210}Pb chronology (Sn0; Sn1) The total ^{210}Pb ($^{210}Pb_{tot}$) activity concentration versus profile depth is presented in Supplementary Table 1. The supported part ($^{210}Pb_{sup}$) was obtained as the mean value (±SD, 1σ) of activities for the lowermost layers, where the level of $^{210}Pb_{tot}$ has reached a steady value. By subtracting $^{210}Pb_{sup}$ activity from $^{210}Pb_{tot}$ activity on a level-by-level basis, the unsupported fraction ($^{210}Pb_{uns}$) was calculated. The average value for $^{210}Pb_{sup}$ fraction was the same for Sn0 and Sn1 and was estimated as 16 ± 3 Bqkg^{-1}. Based on the CF/CS model applied to ^{210}Pb activities, the bottom of Sn0 (50 cm) was dated to 1931 ± 8 CE, and the Sn1 (51 cm) was dated to 1927 ± 5 CE. Thus, the cores encompassed 90 ± 8 y and 86 ± 5 y, respectively. The linear accumulation rates in Sn0 and Sn1 were 0.65 ± 0.11 cm y^{-1} and 0.53 ± 0.04 cm y^{-1}, respectively, and the mass accumulation rate r was 0.020 ± 0.002 g cm^{2}y^{-1} and 0.035 ± 0.002 g cm^{2}y^{-1}, respectively. ^{210}Pb-derived dates from ombrotrophic peat deposits are always validated by independent evidence such as pollution records or other radioisotopes, including $^{239+240}$Pu, ^{241}Am (e.g.,

Appleby et al., 1997; Mackenzie et al., 1998; Gallagher et al., 2001; Cwanek et al., 2021) because decreasing with depth ^{210}Pb activity provided older than expected data. ^{210}Pb dating of peat has been suggested to be unreliable in some studies (e.g., Urban et al., 1990), especially when the CRS model is used (Mróz et al., 2017; Cwanek et al., 2021). Both models (CF=CRS and CF/CS) were used to calculate the ages, but the CRS model gave very old ages for the bottom layers (1828 ± 10 CE for 44.5 cm compared to CF/CS 1941 ± 7 (Supplementary Table 1). For the peat layers dated with Pu at 1952 (the appearance of plutonium in the environment) in core Sn0 and Sn1, the CF/CS model gave 1949 ± 7 CE and 1948 ± 4 CE, while the CRS model provided much older dates of 1900 ± 2 CE and 1921 ± 1 CE, respectively. Similarly, the layers corresponding to the maximum of ^{239,240}Pu concentrations reflecting the peak fallout of 1963 were better dated with the CF/CS model.

The main distinction between the two models is that CF/CS assumes a constant atmospheric flux of ^{210}Pb to the sediment surface and a constant sediment accumulation rate. In contrast, CRS assumes a constant atmospheric flux of ^{210}Pb and a variable accumulation rate of sediments (Supplementary Table 1, Figs. 7 and 8).

3.4 Trace elements (Sn1 and Sn2) The contents of Pb, Zn, Cu, Ni, Cr, Sr, Ti, and Al in Sn1 and Sn2 cores, as well as REE in Sn1 core, were first discussed in Fiałkiewicz et al. (2020), where all elements represented a similar pattern of distribution. Further discussion

in the current paper is centred on Pb, Zn, U, Sc, Al, REE, and S (Fig. 4) for their well-documented linkages with anthropogenic activity and the ability for long-range atmospheric transport (Steinnes and Friedland, 2006). Pb, Zn and U are known to be released by industrial processes (Shotyk et al., 1998; De Vleeschouwer et al., 2010a), S was an important component of acid rain (Mylona, 1996), while Sc, Al, and REE carry the information on dust supply to the peatland (Shotyk et al., 2002; Kylander et al., 2007). For better profile documentation, only concentrations are shown in the figures. However, it should be mentioned that it is crucial to calculate accumulation rates using the age-depth model and bulk density values for a better interpretation of observed variability in the concentrations. Normalised results allow for excluding the effect of some post-depositional processes in the peatland.

Regarding chemical composition, the Sn1 profile was divided into two layers. From ~ 62.5-45.5cm (1795-1952 CE) – with an increase of Pb concentration – up to 220 mg kg^{-1} (62.5cm; 49.5cm). A slight increase of Zn is observed from 59.5 cm (1828 CE). An increase in REE is observed from 52.5-57.5 cm (Fig. 4).

In Sn2, despite partial disturbance of the investigated profile, the distinction of the two layers is also possible (Fig. 4). According to the age-depth model, the layer spanning period similar to Sn1 and Sn0 is 43.5 cm (1899 CE) to the top of the profile. The increase in Pb and S is observed from 31.5 cm (1937 CE), and a slight rise is distinguished in U concentration (33.5 cm – 1928 CE).

3.5 Hg (Sn0) In the Sn0 core, mercury concentration (Fig.8) shows a gradual increase from around 70 ng g^{-1} at the core base to the maximum level of 228 ng g^{-1} in 30.5 cm (1966 CE) and then declines upward to a value of over 40 ng g^{-1}, with some minor fluctuations (Fig. 8). A significant 1950s upturn in Hg concentration is observed at 36.5 cm (1953 CE).

3.6 Pb isotopes (Sn1, Sn2) Pb isotopic ratios are presented in Fig. 4. In both Sn1 and Sn2 profiles, $^{206}Pb/^{207}Pb$ altered from more to less radiogenic value, reaching 1.160-1.162 during the time of the highest detected concentration of all elements. The ash content and chronology revealed disturbances and hiatuses in Sn2. However, the 27.5-0 cm layer, the most important for the Anthropocene, seems reliable and coherent. Lead isotopic signatures revealed similar age and depth patterns in peat profiles during the last 100 years. The observed more complex pattern of Pb isotopic signature in Sn1 might be due to different, higher resolution data, which show variations linked to different sources of Pb associated with changes in wind direction.

3.7 C, N, $\delta^{13}C$, $\delta^{15}N$ (Sn0) The TOC, TN, $\delta^{13}C$, and $\delta^{15}N$ values are shown in Fig. 8. With depth, there is a long-term enrichment in ^{13}C as shown by the $\delta^{13}C$ values (from about -24 to -28.5‰), but from the surface to the first 8cm there is a ^{13}C depletion

(-25.7‰ to -28.5‰). **δ** ^{15}N values also show a long-term enrichment from around -7 to -1‰ in the oldest part of the core. TOC values remain constant with depth while TN values show a significant decrease in the first 8 cm. TN values show a significant drop from 1.2 to 0.4 in the first 8cm and then fluctuate between 0.4 and 1. C:N ratios increase in the first 8cm from 35 to 90 and then fluctuate between 90 and 40.

3.8 Technofossils

SCP (Sn0) The SCPs appeared in the record at 44 – 45cm (approximately 1939 ± 7 CE) (Fig. 8) and occurred continuously above 42 – 43 cm (1943 ± 7 CE) to 8 – 9 cm (2012 ± 1 CE). No SCPs were found in the upper 8 cm of the core.

SAP (Sn0, Sn1, Sn2) Spheroidal aluminosilicates fly ash particles (SAP) were the dominant technogenic dust particles detected in the profiles using SEM. In Sn0, SAPs were first found at a depth of 45 cm (1939±7 CE) (Fig.8), in Sn1 at 40 cm (1950±4 CE), and in Sn2 at 27 cm (1950 CE) (Fig. 4). The size of SAP was analyzed for the Sn0 and Sn1 profiles. Most of the SAP at different depths were <1-9.5µm, which indicates the predominance of SAPs from long-range transport (Smieja-Król and Fiałkiewicz-Kozieł, 2014). A mean SAP size of 2.2 µm was obtained for Sn0 (n=300) and 2.4 µm (n=180) in Sn1. A small number (<2%) of much larger (10-50 µm), less regular, and highly porous technogenic aluminosilicates found within a depth range of 35–25 cm in Sn1 (1961-1983

CE) were probably from local sources. Mullite, an aluminosilicate ($Al_6Si_2O_{13}$) by-product of coal combustion in high temperatures (>1100°C; Smieja-Król et al., 2019), was detected in all profiles (Figs 4, 7, and 8) using XRD. In Sn0, mullite was detected between 13-41 cm (1947-2003 CE), with elevated contents between 22-36 cm (1955-1988 CE) and a maximum at 26-27cm. In Sn1, the range of mullite occurrence was similar, between 12 and 40 cm (1952-2005 CE), with two distinct maxima at 25-26 and 32-33cm. In Sn2, the mullite was only identified in a relatively narrow depth range between 9 and 26 cm. The two maxima were at 15-16 and 18-19 cm.

3.9 Biotic proxies (Sn1) The biostratigraphy was based on pollen, non-pollen palynomorphs, microcharcoal, and testate amoebae (Sn1) (Figs 5 and 6). The proxies revealed three main ecological phases of the peatland with different local and regional agricultural and pastoral activities.

Pollen spectra revealed alpine and upper montane forests in the vicinity of the Śnieżka coring sites. Alpine vegetation was represented by the predominance of herbaceous plants (Poaceae) and high shares of *Pinus sylvestris, Betula alba,* and *Picea abies*. The upper montane forest was indicated by *Pinus mugo* pollen grains. High values of Cerealia type indicate enhanced agricultural activity in the mountain valleys (Fig. 5). In terms of Anthropocene, the most pronounced changes in vegetation are marked by the decline of coprophilous fungi percentages and a gradual increase in *Urtica* values. The decline of

coprophilous fungi indicates a decline in pastoral activity. In contrast, the increase in *Urtica* pollen percentages may be linked to further nitrification of peatland from the input of industrial dust. From ca. 1956 CE (37.5 cm), a continuous presence of pollen of *Ambrosia artemisifolia* type was observed (Fig. 5). The microcharcoal analysis revealed a pronounced upturn at 49.5 cm (1927 CE), keeping the increasing trend till 19.5 cm (1995 CE).

Regarding the testate amoebae, the continuous high abundance of the mixotrophic species *Archerella flavum* and *Hyalosphenia papilio* were observed till 37.5 cm (1956 CE). This was followed by the disappearance of mixotrophs at 36.5 cm (1959±3 CE) and the appearance of dry habitat indicators such as *Alabasta militaris*, *Nebela tincta* and *Galeripora catinus* (drop in the water table, mean DWT value: 26 cm) was recognised (Fig. 6).

The shift between biotic proxies is clearly visible in the non-metric multidimensional scaling (NMDS) 's ordination space (Fig. 9). The most significant variables influencing the communities have been water table depth (Pr(>r): 0.001), Fe (Pr(>r): 0.022) and Pb (Pr(>r): 0.095). The communities typical for the lower part of the peat core were characterised by high abundances of mixotrophic testate amoebae, and the peatland possessed high water tables. Among geochemical data, the presence of Fe and Pb is connected to this phase. The shift in the data set appeared between ca. 1951 and 1965 CE, and the anthropogenically affected communities were dominated by heterotrophic testate

amoeba species. The water table decreased, and plant communities were dominated by *Ambrosia* and *Urtica*.

4. Discussion

4.1. Peat record before 1950' and preferred base for the Anthropocene series

The obtained multi-proxy data of Sn0, Sn1, and Sn2 profiles allows distinction of the boundary between the Holocene and the proposed Anthropocene series encompassing the period of overwhelming human pressure on the environment, called the Anthropocene. Geochemical and paleoecological data consistently indicate that the period between 1795 and 1948±4 CE (63.5 cm to 41.5 cm – for Sn1 and 47.5- 26.5 cm – for Sn2) was characterised by moderate industrial activity in the region. This is confirmed by relatively low Pb accumulation rates (8-20 mg m^{-2} y^{-1}), accompanying high concentrations of Pb in peat (100 – 220 mg kg^{-1} in Sn1) as well as less radiogenic Pb isotopic signatures (1.174-1.160). Zn concentrations were low, albeit displaying an increasing trend during this period, and only at the end of the 19th century (around 1897 CE; 52.5cm) was a considerable increase in Zn accumulation rate from 2.5 to 7 mg m^{-2} y^{-1}. From pollen data, it emerged that the Sudetes mountains were prone to intensifying deforestation, although the predominant land use type was arable farming and pastoralism. The low fluxes of microcharcoal (60 particles $cm^{-2}y^{-1}$) (Fig. 5) seem to indicate low emissions of combustion-related dust but also low settlement density in adjacent valleys and

submontane zones, which might affect the appearance of the fire indicator in the peat record (Patterson et al., 1987). Testate amoebae composition (Fig. 6), with high shares of mixotrophic species *Archerella flavum* or *Hyalosphenia papilio* provided evidence for wet conditions (i.e., higher groundwater level) in the mire.

The year 1948±4 CE (the first global Pu fallout in 1952) appears to be a tipping point in the Śnieżka peatland history (Figs 7, 8, and 9). In the three cores, this date is marked by sharp changes in the deposition of multiple independent geochemical markers of diverse human activities such as fossil fuel combustion, industrialization, and nuclear weapon tests superimposed on climatically driven environmental changes. The first worldwide appearance of Pu (UNSCEAR, 2000; Koide et al., 1979; Krey, 1968) can be recognized globally in different natural archives, including peatlands (Waters et al., 2015). Owing to its synchronicity, Pu is considered a primary marker of the onset of the Anthropocene (Waters et al., 2018; Head et al., 2021).

The appearance of Pu is accompanied by the pronounced inflection (acceleration) or significant upturn of other chemostratigraphic and selected biostratigraphic indicators as well as technogenic particles (SCP, SAP, and mullite), which appeared in the pre-Anthropocene deposits as traces. The NMDS solution (Fig.9) showed low stress values (0.1060076) and proved that the shift in testate amoeba groups (mixotrophs vs. heterotrophs), plant macrofossils and main pollen types appeared in the 1950s, further supporting this period as the border for the Anthropocene series. The markers, crucial in

presenting global patterns in the geological record, were divided into three globally identified categories, i.e., primary markers, technogenic impacts, and climate change, represented here by specific, regional examples of indicators.

4.2. Primary markers The atmospheric deposition of $^{239+240}$Pu in the Śnieżka cores correlates with global events in the history of radioactive fallout, notably coupled to thermonuclear atmospheric weapons testing from 1952 and the Partial Test Ban Treaty signed in 1963 (Figs 3, 7, and 8). Plutonium isotopes (^{238,239,240}Pu) are useful independent chronostratigraphic markers due to long half-lives of 24,100 (^{239}Pu) and 6561 years (^{240}Pu), respectively. They are characterized by low solubility and high stability in peatlands, as Pu is retained by *Sphagnum* mosses (Testa et al., 1999; Waters et al., 2015). There is a 2-cm difference between the first appearance of $^{239+240}$Pu in Sn1 and Sn0, caused by different dynamics of peat growth. Nevertheless, the high repeatability between the two profiles confirms the immobility of Pu in the presented stratigraphic record (Figs 3, 7, and 8). We may summarise that the highest extended peak of $^{239+240}$Pu activity concentrations dated to 1965 ± 3 CE for Sn1 and 1966 ± 5 CE for Sn0 (CF/CS) were the consequences of the most intensive period of nuclear weapons testing and a further moratorium in the 1960s.

Due to Pu immobility, the historical data of the first global fallout should be attributed to the layer of 1952 CE, which is consistent with ages modelled by the ^{210}Pb method.

1952-peaks are observed at the 41.5 cm depth (1948 ± 4 CE) for Sn1 and 39.5 cm depth (1949 ± 6 CE) for Sn0 (Figs 3, 4, 5, 6, Supplementary Table 1). Below 1952 in both profiles, we observed small peaks dated 1941 for Sn0 and 1936 for Sn1. The presence of the global fallout derived Pu at depth-ages preceding 1952 is probably evidence of the post-depositional migration of Pu vertically downwards, also observed by others in peat profiles (Quinto et al., 2013; Kazakevičiūtė-Jakučiūnienė et al., 2022). However, the extent of the mobility is much smaller than for Cs, thus not significantly affecting the age-depth models based on Pu profiles. The shift in the levels of the $F^{14}C$ for Sn0 (Fig. 10) compared with the atmospheric curve NH1 (Hua et al., 2021) revealed a great similarity to the Pu curve plotted vs. ^{210}Pb model, confirming the robustness of the used modelling. The peaks of $^{239,240}Pu$ in Sn0 and Sn1 profiles also correspond well with the main peaks of ^{137}Cs (Fig. 3).

The peak concentrations of ^{137}Cs are slightly shifted in depth with respect to the peaks of plutonium. In profile Sn1, the maximum of the ^{137}Cs activity is observed in the top layer, which could be attributed to the active uptake by living plants (e.g., Rosen et al., 2009; Mróz et al., 2017). However, the Chernobyl peak (1986) of ^{137}Cs is partly preserved. Profil Sn0 is less affected by plant uptake of Cs, which corresponds with a less dense plant cover at the Sn1 sampling site. Also, the Chernobyl peak is more distinct. Measurable ^{137}Cs activity was found in all layers of both profiles, pointing to the downward mobility of Cs. The mobility of ^{137}Cs in ombrotrophic peat bogs (Olid et al.,

2008; Zaccone et al., 2007) is due to the lack of suitable mineral particles for the adsorption of alkali metal cations like Cs.

Some vertical mobility of ^{137}Cs in ombrotrophic peat deposits is demonstrated in Sn0 and Sn1 and is also observed in other sites (e.g., Mitchell et al., 1992; Mackenzie et al., 1997; Mroz et al., 2017; Fiałkiewicz-Kozieł et al., 2014; Rosen et al., 2009; Kazakevičiūtė-Jakučiūnienė et al., 2022). ^{137}Cs could be immobile (Li et al., 2017; Łokas et al., 2013; van der Plicht et al, 2013) or partially mobile downward and upward in the peat profile (Schell et al., 1989) due to biological activity in the root zone and changing water table (Rosen et al., 2009; Aaby et al., 1979). Nevertheless, it was possible to recognise the most characteristic events of radionuclide fallout, i.e., Chernobyl accident.

4.3. The technogenic impact: synchronous increases of chemical elements concentration and associated appearance of SCP and SAP, mullite, δ^{15}N, and δ^{13}C

The increased global human population and their energy demands have induced a dramatic increase in the number of power plants, industrial facilities, car use, and associated fossil fuel combustion (Waters et al. 2016; 2018). Fossil fuel-based power plants and industrial activities emit flue gases and fly-ashes (e.g., Vassilev et al., 2001; Jones et al., 2012). These are transported in the atmosphere before they are deposited on aquatic and terrestrial surfaces, including different natural archives.

Ombrotrophic peatlands are among the best archives of rare and trace elements deposition due to being fed only from the atmosphere and the effective immobilisation of selected elements, once deposited, which can be interpreted against an age-depth function (Shotyk, 1988; De Vleeschouver et al., 2010a). In Śnieżka peatland, trace elements were determined in Sn1 and Sn2, but the simultaneous increase in ash content of Sn1 and Sn2, which correlates with peaks in element concentrations, also allows for the recognition of such a layer in ash content in Sn0. Hence, Sn0 ash content may be considered equivalent to chemical element deposition and, in particular, corresponds with the profile of mercury content and accumulation (Fig. 8).

Trace elements Pb and Zn are representative of industrial activity and so may be used in the discussion regarding markers for the Anthropocene series. Numerous studies have identified ombrotrophic bogs as among the best Pb archives due to their exclusive input via deposition from the atmosphere (e.g., Shotyk et al., 1998; Shotyk et al., 2005). Pb always accompanies Zn in peat because of their co-occurrence in ore deposits (De Vleeschouver et al., 2009; Smieja-Król et al., 2010). Despite its mobility in peatlands (Weiss et al., 2002), Zn deposition shows similar patterns to Pb in the Śnieżka cores (Fig. 4; Fiałkiewicz-Kozieł et al., 2020).

Comparison of industrially driven Pb deposition in archives from different countries and continents indicates regional or local differences due to the individual history of industrial development (Longman et al., 2020). However, despite significant intracontinental

variability, the most pronounced increase, observed in the mid-20th century, has been statistically confirmed (Longman et al., 2020). This has important implications for determining a clear boundary for the Anthropocene series using trace elements. While peat sequences in different countries may show varying dates for the onset of trace metal contamination and for peak metal concentrations making them unsuitable as a global synchronous marker, the rise in trace metal inputs for Pb and Zn in the 1950s does appear to be globally synchronous for all studied peat deposits. This increase in almost all investigated trace elements and REE is visible in Śnieżka peatland (Fiałkiewicz-Kozieł et al., 2020) and here may be attributed to lignite combustion in 'Black Triangle' countries (Fiałkiewicz-Kozieł et al., 2015; 2020). The 1950s acceleration in Pb is observed in different environmental archives, for example, in Czechia (Novak et al., 2008), Scotland (Farmer et al., 2007), Greenland (Shotyk et al., 2003), but also China (Bao et al., 2015; Fiałkiewicz-Kozieł et al., 2022) and Kyrgyzstan (Griholm et al., 2016). This "Great Acceleration" in chemical element inputs due to increased industrial activity is given here as one of the significant markers of the proposed Anthropocene.

Technofossils High-temperature coal combustion also produces technofossils like spheroidal carbonaceous particles (SCP) or fly ash spheroidal aluminosilicates (SAP), easily detected in peat profiles (Rose, 2015; Swindles, 2015; Smieja-Król and Fiałkiewicz-Kozieł, 2015; Fiałkiewicz-Kozieł et al., 2020 - for this study). SCPs and

SAPs appeared for the first time in western Europe in the mid-19th century, but the marked global increase in abundance is observed around 1950 CE, with peak inputs to archives ranging regionally from the 1970s–to the 1990s (Rose, 2015; Smieja-Król et al., 2019). The link with specific technology, developed in the late 19th century and boosted in the 1950s-1960s allows for the determination of distinct boundaries in the geological record, even at remote sites far from industrial centres (Fiałkiewicz-Kozieł et al., 2016, 2022). In Śnieżka, the first appearance is observed in 1940 CE; however, a significant upturn is visible in the 1950s (Figs 7 and 8).

Stable isotopes Stable carbon ($\delta^{13}C_{TOC}$) and nitrogen ($\delta^{15}N$) isotope signatures can, with some limitations, also be used to show the anthropogenic contribution of carbon and nitrogen deposition on the Śnieżka peatland. Both $\delta^{13}C_{TOC}$ and $\delta^{15}N$ displayed similar patterns (Pearson correlation coefficient r = 0.72, p <<0.001), indicating that the same environmental factors control them. Decreasing trends in $\delta^{13}C$ and $\delta^{15}N$ between the early 1940s CE and 1970s CE reflect a long-term depletion in atmospheric ^{13}C and ^{15}N. For CO_2, the decrease could act as a manifestation of the so-called Suess effect, a worldwide reduction of atmospheric $\delta^{13}C_{CO2}$ values by ~2‰ within the last 200 years due to the burning of fossil fuels (Keeling, 1979; Keeling et al., 1979). The $\delta^{13}C_{TOC}$ and $\delta^{15}N$ trend could indicate that between the 1940s and 1970s CE, there occurred a decline in $\delta^{13}C$ and $\delta^{15}N$ values in atmospheric CO_2 and NO_3, respectively, in the Sudetes.

It should be emphasised that $\delta^{13}C_{OM}$ and $\delta^{15}N$ are known to be strongly influenced by microbial OM degradation, leaching, and refixation in the peat acrotelm, which preferentially removes light C and N isotopes, thus leading to an increase of $\delta^{13}C_{OM}$ and $\delta^{15}N$ in the residual recalcitrant material (Esmeijer-Liu et al., 2012). On the other hand, it has been documented that in the early stages of a microbial attack, ^{13}C enriched carbohydrates are removed, and as a result, the $\delta^{13}C$ of the remaining organic material is shifted towards lower values (Meyers, 1997). Such an effect is presumably responsible for stable C isotope signatures in the uppermost 8 cm-thick layers of the Sn cores (Fig. 8).

4.4 Biotic markers of the Anthropocene series

Pollen analysis The critical changes in elements and technofossils at the proposed Holocene/Anthropocene transition correspond with pronounced ecological changes mirrored by pollen and testate amoebae in the Sn1 profile (Figs 5, 6, and 7). However, while chemical markers and technofossils often have worldwide distributions, the pollen-inferred delimitation of the Anthropocene relies on species that represent region-specific ecological trends (Deza-Araujo et al., 2022). Therefore, representative analogues should be selected from different parts of the globe when comparing these markers. Globalisation phenomena and climate change have altered the distribution of non-native species, which have become invasive in new environments (Storkey et al., 2014). In Europe, one of the

best-known alien plants is *Ambrosia artemisifolia* L. (common ragweed), which has expanded over Europe since 1940 CE due to its contamination within crop seeds and transboundary transport (Chauvel et al., 2006; Storkey et al., 2014). From the Sn1 core, it emerges that in central Europe, *Ambrosia artemisifolia* appeared in 1956±3 CE (Fig.5). An interesting feature of the Sn0 profile was a gradual increase in *Urtica* pollen abundance, which might be an effect of enrichment with nitrogen. A decline in nitrogen input occurred due to the cessation of pastoral activity connected with the establishment of Karkonosze National Park in 1959. However, in the following period, intensified tourism and enhanced atmospheric fallout caused by industrial development in the Black Triangle (Kmiec et al., 1995; Myśkow et al., 2019) partially compensated for this N loss. *Urtica dioica* and *Urtica urens* are characteristic representatives of nitrophilic weeds (Rosnitschek-Schimmel, 1983), and *Urtica* sp. records show an increasing trend from 1950, representative of many European mountain records (Segnana et al., 2020), and a clear connection between its presence and the anthropogenic phase (Fig. 9).

In the Snieżka record, it is also clear that in ca. 1960 CE, there was a considerable change in the microbial food web reflected by the disappearance of mixotrophic testate amoebae (Fig. 6). This change is found to reflect the broader tendency observed in some parts of the Northern Hemisphere: Siberia (Lamentowicz et al., 2015) and Canada (van Bellen et al., 2018) as well as in the Southern Hemisphere (e.g., van Bellen et al., 2016). In all these locations, the collapse in mixtrotrophic species was associated with the lowering of the

water table and shading by shrubs (Heal, 1964; Schönborn, 1965; Lamentowicz and Mitchell, 2005; Marcisz et al., 2014; Payne et al., 2016; Creevy et al., 2018; Lamentowicz et al. 2020). Even though global warming was among the most important drivers of the peatland drying trend during the past 70 years (Gallego Sala et al., 2018), there are alternative reasons for the disappearance of mixotrophs in the Śnieżka bog. It appears that the local testate amoebae communities were exposed to fly ash deposition originating from intense industrial activity around the so-called Black Triangle (Fig. 1), and it has been hypothesised that this dust harmed mixotrophic metabolism and eliminated communities living at the capitula of *Sphagnum* (Fiałkiewicz-Kozieł et al., 2015; Marcisz et al., 2020). Synergistic effects of air pollution and anthropogenic global warming might cause the worldwide extinction of the populations of mixotrophs in *Sphagnum* peatlands in the future (Loisel et al., 2021). By contrast, the Śnieżka peatland has also been identified as the location of new ecotypes of testate amoebae which are resistant to pollution and which use fly-ash particles to build their shells (Fig. 11). The first evidence for this phenomenon was described in the Izery mountains (Fiałkiewicz-Kozieł et al., 2015).

4.5 Śnieżka peatland as potential GSSP Due to the widespread environmental effects of industrial activity in the Black Triangle and the high-resolution record preserved in the peatland, the Śnieżka site seems significant for documenting the Anthropocene. The

unique feature of the site lies in its location in the subalpine zone and at the trajectory of air masses carrying pollutants over long distances across Europe. The Anthropocene series in the Sn cores is clearly distinguished by the distributions of Pu isotopes, technofossils (SCP, SAP, and mullite) as well as trace metals, all of which are synchronous with other Anthropocene records worldwide.

As a candidate for a GSSP representative Anthropocene core, the Sn0 has the following advantages:

- It displays a robust age model obtained using ^{210}Pb and verified by independent markers (^{137}Cs, F^{14}C)
- It is characterised by a relatively high peat accumulation rate (0.66 cm·y^{-1} on average) which provides a high-resolution geological record (around 2 years per 1 cm) and thus allows for the identification of a distinct boundary between the Holocene and Anthropocene series
- The Sn0 peat profile provides a continuous geological record for the last c.a. 100 years (i.e., no hiatuses, gaps, and other disturbances were identified)
- The Sn0 Anthropocene archive encompasses a wide array of critical markers such as plutonium radionuclides, fly ash particles, Hg, and stable C and N isotopes which are consistent with the previously studied well-documented Sn1 profile
- The Śnieżka site is located in a protected area of the National Park and is easily accessible for further studies. Access to the peatland is facilitated thanks to

proximity to touristic tracks, although permission for collecting peat material, given by the Ministry of Climate and Environments and the National Park Administration, is mandatory.

The main disadvantages of the proposed stratotype include the lack of annual lamination and the lack of a lithological marker at the proposed level.

Conclusions The Śnieżka peat profile provides a significant volume of deposited organic matter and presents a comprehensive dataset of markers which can be used to distinguish a 1950s boundary between the Holocene and Anthropocene series. Despite an absence of annual layering the proposed GSSP core has a well-constrained chronology and key markers (Pu, Cs, technofossils) can be correlated to adjacent cores. Importantly, further analysis is required to repeat some crucial measurements undertaken in 2020 - 2022 as part of future examinations of the candidate GSSP core. The proposed name for the stage/age-level is Sudetian.

Acknowledgements

This research was funded by the Polish National Centre of Science (NCN) 2011/01/D/ST10/02579 granted to BFK as well as by IGIG, Adam Mickiewicz University funds for scientific activity. Gael Le Roux is thanked for the discussion about Pu mobility. We would like to acknowledge the Haus der Kulturen der Welt (HKW, Berlin) for

collaborating with the Anthropocene Working Group in the assessment of the candidate GSSP-sites. The collaboration was established in the framework of HKW's long-term initiative Anthropocene Curriculum, an international project for experimental forms of Anthropocene research and education developed by HKW and the Max Planck Institute for the History of Science (MPIWG, Berlin) since 2013. Colin Waters is warmly thanked for all constructive comments.

Figures

1. Map of the study site. The wind rose after Sobik (2014).

2. Results of macrofossil analysis and physical properties of sediments for all investigated cores.

3. Comparison of $^{239+240}$Pu and ^{137}Cs vs. CF/CS modelled dates in Sn0 and Sn1.

4. Geochemistry of Sn1 and Sn2 (based on Fiałkiewicz-Kozieł et al., 2020 except for mullite and sulphur). Sn1 profile records the appearance of 1952-Pu and spheroidal aluminosilicates (SAP) signal, while Sn2 SAP signal only. The chronology is based on the ^{14}C/^{210}Pb model. At a depth of 41.5 cm (Sn1), the date of the first Pu appearance is provided, not measured in Sn2.

5. Simplified pollen diagram for Sn1 profile. 10 x exaggeration provided for better visualisation. At a depth of 41.5 cm, the date of the first Pu appearance is provided.

6. Short percentage diagram of the most frequent testate amoebae and reconstructed depth to the water table in Sn1 profile. In green - mixotrophs, orange – indicators of dry conditions. 5 x exaggeration provided for better visualisation. At a depth of 41.5 cm, the date of the first Pu appearance is provided.

7. Summary of the most significant markers in Sn1. The horizontal dashed line is referred to first global Pu fallout (1952).

8. Summary of markers in Sn0. The horizontal dashed line is referred to first global Pu fallout (1952).

9. Non-metric multidimensional scaling (NMDS) diagrams for Śnieżka multiproxy dataset. NMDS shows a low-stress value (0.106) for the two-dimensional solution. Reconstructed depth to the water table (DWT) and geochemical data are projected on the ordination space. Codes for pollen types follow the pollen diagram (Fig. 5). Testate amoebae are projected as a sum of mixotrophic species ("TA Mixotrophs") and a sum of heterotrophic species ("TA Heterotrophs").

10. The comparison of $F^{14}C$ values (Sn0) (against ^{14}C age-depth model) with atmospheric curve and with Pu, which is presented against ^{210}Pb model. The overall similarity revealed between two independent models has confirmed the accuracy and robustness of both methods of dating.

11.Fossil shell of a testate amoeba with SAP built into the shell (indicated by red circles) (Sn0, depth 25-26 cm).

References

Aaby B, Jacobsen J, and Jacobsen O S (1979) Pb-210 dating and lead deposition in the ombrotrophic peat bog Draved Mose Denmark. *Danmarks Geologisk Ungersoglse Arbog*, pp 5-43.

Appleby PG, Shotyk W, Fankhauser A (1997) Lead-210 age dating of three peat cores in the Jura Mountains, Switzerland. *Water, Air, and Soil Pollution* 100: 223–231.

AWG (2020) Newsletter vol 10 Anthropocene Working Group of the subcommission on quaternary stratigraphy (International Commission on Stratigraphy). AWG Washington.

Bao K, Shen J, Wang G, Le Roux G (2015) Atmospheric deposition history of trace metals and metalloids for the last 200 years recorded by three peat cores in Great Hinggan Mountain Northeast China. *Atmosphere* 6 (3): 380-409.

Bińczycki T, Weber J, Mielnik L, Asensio C (2020) Lead isotope ratios in Podzol profiles as a tracer of pollution source in the subalpine zone of the Karkonosze National Park Sudety Mts (south-western Poland). *Catena* 189: 104476.

Chauvel B, Dessaint F, Cardinal-Legrand C, Bretagnolle F (2006)The historical spread of Ambrosia artemisiifolia L. in France from herbarium records. *Journal of Biogeography* 33: 665–73.

Creevy AL, Andersen R, Rowson JG, Payne RJ (2018) Testate amoebae as functionally significant bioindicators in forest-to-bog restoration. *Ecological Indicators* 84: 274-282.

Cwanek A, Łokas E, Mitchell EA, Mazei Y, Gaca P, Milton J A (2021) Temporal variability of Pu signatures in a ^{210}Pb-dated Sphagnum peat profile from the Northern Ural Russian Federation. *Chemosphere* 281: 130962.

De Vleeschouwer F, Fagel N, Cheburkin A, Pazdur A, Sikorski J, Mattielli N, Renson V, Fialkiewicz B, Piotrowska N (2009) Anthropogenic impacts in North Poland over the last 1300 years. *Science of the Total Environment* 407: 5674-5684.

De Vleeschouwer F, Le Roux G, Shotyk W (2010a) Peat as an archive of atmospheric pollution and environmental change: A case study of lead in Europe. *PAGES* 18:20-22.

De Vleeschouwer F, Chambers FM, Swindles GT (2010b) Coring and sub-sampling of peatlands for palaeoenvironmental research *Mires and Peat* 7: 1.

Deza - Araujo M, Morales-Molino C, Conedera M, Pezzatti GB, Pasta S, Tinner W (2022) Influence of taxonomic resolution on the value of anthropogenic pollen indicators. *Vegetation History and Archaeobotany* 31: 67–84.

Esmeijer-Liu AJ, Kürschner WM, Lotter AF (2012) Stable carbon and nitrogen isotopes in a peat profile are influenced by early stage diagenesis and changes in atmospheric CO2 and N deposition. *Water Air Soil Pollution* 223: 2007–2022.

Farmer JG, MacKenzie AB, Sugden CL, Edgar PJ, Eades LJ (1997) A comparison of the historical lead pollution records in peat and freshwater lake sediments from central Scotland. *Water Air and Soil Pollution* 100: 253-270.

Fiałkiewicz-Kozieł B, Kołaczek P, Piotrowska N, Michczyński A, Łokas E, Wachniew P, Woszczyk M, Sensuła B (2014) High-resolution age-depth model of a peat bog in Poland as an important basis for paleoenvironmental studies. *Radiocarbon* 56: 109–125.

Fiałkiewicz-Kozieł B, Smieja-Król B, Ostrovnaya TM, Frontasyeva M, Siemińska A, Lamentowicz M (2015) Peatland Microbial Communities as Indicators of the Extreme Atmospheric Dust Deposition. *Water Air and Soil Pollution* 226: 97-103.

Fiałkiewicz-Kozieł B, Smieja-Krol B, Frontasyeva M, Slowinski M, Marcisz K, Lapshina E, Gilbert D, Buttler A, Jassey VE, Kaliszan K, Laggoun-Defarge F, Kolaczek P, Lamentowicz M (2016) Anthropogenic- and natural sources of dust in peatland during the Anthropocene. *Scientific Reports* 6: 38731.

Fiałkiewicz-Kozieł B, De Vleeschouwer F, Mattielli N, Fagel N, Palowski B, Pazdur A, Smieja-Król B (2018) Record of Anthropocene pollution sources of lead in disturbed peatlands from Southern Poland. *Atmospheric Environment* 179: 61-68.

Fiałkiewicz – Kozieł B, Łokas E, Gałka M, Kołaczek P, De Vleeschouwer F, Le Roux G, Smieja-Król B (2020) Influence of transboundary transport of trace elements on mountain peat geochemistry (Sudetes Central Europe). *Quaternary Science Reviews* 230: 106162.

Fiałkiewicz-Kozieł B, Bao K, Smieja-Król B (2022) Geographical drivers of geochemical and mineralogical evolution of Motianling peatland (Northeast China) exposed to different sources of rare earth elements and Pb Nd and Sr isotopes. *Science of The Total Environment* 807: 150481.

Gallagher D, McGee E J, Mitchell P I (2001) A recent history of 14C, 137Cs, 210Pb and 241Am accumulation at two Irish peat bog sites: an east versus west coast comparison. *Radiocarbon* 43(2B): 517-525.

Gallego-Sala AV, Charman DJ, Brewer S, Page SE, Prentice IC, Friedlingstein P, Moreton S, Amesbury MJ, Beilman DW, Björck S, Blyakharchuk T, Bochicchio C, Booth RK, Bunbury J, Camill P, Carless D, Chimner RA, Clifford M, Cressey E, Courtney-Mustaphi C, De Vleeschouwer F, de Jong R, Fialkiewicz-Koziel B, Finkelstein SA, Garneau M, Githumbi E, Hribjlan J, Holmquist J, Hughes PDM, Jones C, Jones MC, Karofeld E, Klein ES, Kokfelt U, Korhola A, Lacourse T, Le Roux G, Lamentowicz M, Large D, Lavoie M, Loisel J, Mackay H, MacDonald GM, Makila M, Magnan G, Marchant R, Marcisz K, Martínez Cortizas A, Massa C, Mathijssen P, Mauquoy D, Mighall T, Mitchell FJG, Moss P, Nichols J, Oksanen PO, Orme L, Packalen MS, Robinson S, Roland TP, Sanderson NK, Sannel ABK, Silva-Sánchez N, Steinberg N, Swindles GT, Turner TE, Uglow J, Väliranta M, van Bellen S, van der Linden M, van Geel B, Wang G, Yu Z, Zaragoza-Castells J, Zhao Y (2018) Latitudinal limits to the predicted increase of the peatland carbon sink with warming. *Nature Climate Change* 8: 907-913.

Givelet N, Le Roux G, Cheburkin A, Chen B, Frank J, Goodsite ME, Kempter H, Krachel M, Noernberg T, Rausch N, Rheinberger S, Roos-Barraclough F, Sapkota A, Scholz Ch, Shotyk W (2004) Suggested protocol for collecting handling and preparing

peat cores and peat samples for physical chemical mineralogical and isotopic analyses. *Journal of Environmental Monitoring* 6: 481-492.

Glina B, Bogacz A (2013) Concentration and pools of trace elements in organic soils in the Izera Mountains. *Journal of Elementology* 18(2):199-209.

Grübler A (2002) Trends in global emissions: carbon, sulphur and nitrogen. In: Douglas(ed) IIASA Laxenburg Austria, pp. 35–53.

Hajdas I (2008) The Radiocarbon dating method and its applications in Quaternary studies. *Quaternary Science Journal - Eiszeitalter und Gegenwart* 57(1/2):2-24.

Hansson SV, Claustres A, Probst A, de Vleeschouwer F, Baron S, Galop D, Mazier F, Le Roux G (2017) Atmospheric and terrigenous metal accumulation over 3000 years in a French mountain catchment: Local vs distal influences. *Anthropocene* 19: 45-54.

Head MJ, Steffen W, Fagerlind D, Waters CN, Poirier C, Syvitski J, Zalasiewicz JA, Barnosky AD, Cearreta A, Jeandel C, Leinfelder R, McNeill JR, Rose NL, Summerhayes C, Wagreich M, and Zinke J (2021) The Great Acceleration is real and provides a quantitative basis for the proposed Anthropocene series/Epoch. *Episodes*.

Heal OW (1964) Observations on the Seasonal and Spatial-Distribution of Testacea (Protozoa Rhizopoda) in Sphagnum. *Journal of Animal Ecology* 33: 395-412.

Hua Q, Turnbull JC, Santos GM, Rakowski AZ, Ancapichún S, De Pol-Holz R, Hammer S, Lehman SJ, Levin I, Miller JB, Palmer JG, Turney CSM (2021) Atmospheric Radiocarbon for the Period 1950–2019. *Radiocarbon*: 1-23.

Jones KB, Ruppert LF, Swanson SM (2012) Leaching of elements from bottom ash economizer fly ash and fly ash from two coal-fired power plants. *International Journal of Coal Geology* 94: 337–348.

Julkowska V (2006) Cultural heritage as the heritage of memory. *Historia a teoria* 1: 7-9.

Kajukało K, Fiałkiewicz-Kozieł B, Gałka M, Kołaczek M, Lamentowicz M (2016) Abrupt ecological changes in the last 800 years inferred from a mountainous bog using testate amoebae traits and multi-proxy data. *European Journal of Protistology* 55:165-180.

Kazakevičiūtė-Jakučiūnienė L, Tarasiuk N, Maceika E, DruteikienėR, Ežerinskis Ž, Šapolaitė J, Žukauskaitė Z, Gvozdaitė R (2022) Analysis of the vertical distribution of ^{137}Cs and ^{239,240}Pu in waterlogged and non-boggy soils by the sequential extraction method. *Journal of Environmental Radioactivity* 253: 106990.

Keeling CD (1979) The Suess effect: ^{13}Carbon-^{14}Carbon interrelations. *Environment International* 2:229–300.

Keeling CD, Mook WG, Tans PP (1979) Recent trends in the $^{13}C/^{12}C$ ratio of atmospheric carbon dioxide. *Nature* 277:121–123.

Kmiec G, Kacperczyk K, Zwozdziak A, Zwozdziak J (1995) Acid pollutants in air and precipitation/deposition at the Sudeten Mountains, Poland. *Water Air and Soil Pollution* 85: 2131-2136.

Koide M, Michel R, Goldberg ED, Herron MM, Langway Jr CC (1979) Depositional history of artificial radionuclides in the Ross Ice Shelf Antarctica. *Earth and Planetary Science Letters* 44: 205-223.

Kolář T, Čermák P, Oulehle F, Trnka M, Štepánek P, Cudlín P, Hruška J, Büntgen U, Rybníček M (2015) Pollution control in the 1980s contributed to unprecedented spruce growth in the "BlackTriangle" The Czech-Polish Border region. *Science of the Total Environment* 538: 703–711.

Krey PW (1967) Atmospheric burnup of a plutonium-238 generator. *Science* 84158: 769–771.

Kylander ME, Muller J, Wüst RA, Gallagher K, Garcia-Sanchez R, Coles BJ, Weiss DJ (2007) Rare earth element and Pb isotope variations in a 52 kyr peat core from Lynch's crater (NE Queensland Australia): proxy development and application to paleoclimate in the southern hemisphere. *Geochimica et Cosmochimica Acta* 71: 942-960.

Lamentowicz M, Kajukało-Drygalska K, Kołaczek P, Jassey VEJ, Gąbka M, Karpińska-Kołaczek M (2020) Testate amoebae taxonomy and trait diversity are coupled along an openness and wetness gradient in pine-dominated Baltic bogs. *European Journal of Protistology* 73: 125674

Lamentowicz M, Mitchell EAD (2005) The ecology of testate amoebae (Protists) in *Sphagnum* in north-western Poland in relation to peatland ecology. *Microbial Ecology* 50: 48-63.

Lamentowicz M, Słowiński M, Marcisz K, Zielińska M, Kaliszan K, Lapshina E, Gilbert D, Buttler A, Fiałkiewicz-Kozieł B, Jassey VEJ, Laggoun-Defarge F, Kołaczek P (2015) Hydrological dynamics and fire history of the last 1300 years in Western Siberia reconstructed from a high-resolution ombrotrophic peat archive. *Quaternary Research* 84: 312-325.

Li C, Le Roux G, Sonke J, van Beek P, Souhaut B, Van der Putten N, De Vleeschouwer F (2017) Recent ^{210}Pb, ^{137}Cs and ^{241}Am accumulation in an ombrotrophic peatland from Amsterdam Island (Southern Indian Ocean). *Journal of environmental radioactivity* 175: 164-169.

Loisel J, Yu Z, Beilman D, Camill P, Alm J, Anderson D, Andersson S, Fiałkiewicz-Kozieł B, Barber K, Belyea L, Bunbury J, Chambers F, Charman D, de Vleeschouwer F, Finkelstein S, Garneau M, Hendon D, Holmquist J, Hughes P, Jones M, Klein E, Kokfelt U, Korhola A, Kuhry P, Lamarre A, Lamentowicz M, Large D, Lavoie M, MacDonald G, Magnan G, Gałka M, Mathijssen P, Mauquoy D, McCarroll J, Moore T, Nichols J, O'Reilly B, Oksanen P, Peteet D, Richard P, Robinson S, Rundgren M, Sannel B, Tuittila ES, Turetsky M, Valiranta M, van der Linden M, van Geel B, van Bellen S, Vitt D, Zhao Y, Zhou W (2014) A synthesis of existing data for northern peatland soil properties and Holocene carbon accumulation. *Holocene* 24 (9): 1028-1042.

Loisel J, Gallego-Sala AV, Amesbury MJ, Magnan G, Anshari G, Beilman DW, Benavides JC, Blewett J, Camill P, Charman DJ, Chawchai S, Hedgpeth A, Kleinen T,

Korhola A, Large D, Mansilla CA, Müller J, van Bellen S, West JB, Yu Z, Bubier JL, Garneau M, Moore T, Sannel ABK, Page S, Väliranta M, Bechtold M, Brovkin V, Cole LES, Chanton JP, Christensen TR, Davies MA, De Vleeschouwer F, Finkelstein SA, Frolking S, Gałka M, Gandois L, Girkin N, Harris LI, Heinemeyer A, Hoyt AM, Jones MC, Joos F, Juutinen S, Kaiser K, Lacourse T, Lamentowicz M, Larmola T, Leifeld J, Lohila A, Milner AM, Minkkinen K, Moss P, Naafs BDA, Nichols J, O'Donnell J, Payne R, Philben M, Piilo S, Quillet A, Ratnayake AS, Roland TP, Sjögersten S, Sonnentag O, Swindles GT, Swinnen W, Talbot J, Treat C, Valach AC, Wu J (2021) Expert assessment of future vulnerability of the global peatland carbon sink. *Nature Climate Change* 11: 70-77.

Łokas E, Mietelski JW, Ketterer ME, Kleszcz K, Wachniew P, Michalska S, Miecznik M (2013) Sources and vertical distribution of ^{137}Cs ^{238}Pu $^{239+240}$Pu and ^{241}Am in peat profiles from southwestern Spitsbergen. *Applied Geochemistry* 28: 100-108.

Longman J, Ersek V, Veres D (2020) High variability between regional histories of long-term atmospheric Pb pollution. *Scientific Reports* 10: 20890.

Luciano E (2022) Is 'Anthropocene' a Suitable Chronostratigraphic Term? *Anthropocene Science* 1: 29-41.

MacKenzie AB, Farmer JG, Sugden CL (1997) Isotopic evidence of the relative retention and mobility of lead and radiocaesium in Scottish ombrotrophic peats. *Science of the Total Environment* 203(2): 115-127.

MacKenzie AB, Logan EM, Cook GT, Pulford ID (1998) Distributions inventories and isotopic composition of lead in ^{210}Pb-dated peat cores from contrasting biogeochemical environments: implications for lead mobility. *Science of the Total Environment* 223(1): 25-35.

Magiera T, Żogała B, Szuszkiewicz M, Pierwoła J, Szuszkiewicz MM (2019) Combination of different geophysical techniques for the location of historical waste in the Izery Mountains (SW Poland). *Science of the Total Environment* 682: 226-238.

Marcisz K, Jassey VEJ, Kosakyan A, Krashevska V, Lahr DJG, Lara E, Lamentowicz Ł, Lamentowicz M, Macumber A, Mazei Y, Mitchell EAD, Nasser NA, Patterson RT, Roe HM, Singer D, Tsyganov AN, Fournier B (2020) Testate Amoeba Functional Traits and Their Use in Paleoecology *Frontiers in Ecology and Evolution* 8: 340.

Marcisz K, Lamentowicz Ł, Słowińska S, Słowiński M, Muszak W, Lamentowicz M (2014) Seasonal changes in Sphagnum peatland testate amoeba communities along a hydrological gradient. *European Journal of Protistology* 50: 445-455.

Mazurski KR (1986) The destruction of forests in the Polish Sudetes Mountains by industrial emissions. *Forest Ecology and Management* 17:303-315

Meyers PA (1997) Organic geochemical proxies of paleoceanographic, paleolimnologic and plaeoclimatic processes. *Organic Geochemistry* 27:213–250.

Millar DJ, Cooper DJ, Dwire KA, Hubbard RM, von Fischer J (2017) Mountain Peatlands Range from CO_2 Sinks at High Elevations to Sources at Low Elevations:

Implications for a Changing Climate. *Ecosystems* 20: 416–432.

Mitchell G, McDonald A T (1992) Discolouration of water by peat following induced drought and rainfall simulation. *Water Research* 26(3): 321-326.

Mróz T, Łokas E, Kocurek J, Gąsiorek M (2017) Atmospheric fallout radionuclides in peatland from Southern Poland. *Journal of environmental radioactivity* 175 25-33.

Mylona S (1996) Sulphur dioxide emissions in Europe 1880–1991 and their effect on sulphur concentrations and depositions. *Tellus* B 48 (1): 662-689.

Myśkow E, Błaś M, Sobik M, Godek M, Owczarek P (2019) The effect of pollutant fog deposition on the wood anatomy of subalpine Norway spruce. *European Journal of Forest Research* 138: 187–201.

Nemec M, Wacker L, Gaggeler H (2010) Optimization of the Graphitization Process at Age-1. *Radiocarbon* 52(3): 1380-1393.

Novak M, Brizova E, Adamova M, Erbanova L, Bottrell SH (2008) Accumulation of organic carbon over the past 150 years in five freshwater peatlands in western and central Europe. *Science of the Total Environment* 390(2-3): 425-436.

Oldfield F, Richardson N, Appleby P G (1995) Radiometric dating (^{210}Pb, ^{137}Cs, ^{241}Am) of recent ombrotrophic peat accumulation and evidence for changes in mass balance. *The Holocene* 5(2): 141-148.

Olid C, Garcia-Orellana J, Martinez-Cortizas A, Masque P, Peiteado E, Sanchez-Cabeza JA (2008) Role of Surface Vegetation in Pb-210-Dating of Peat Cores. *Environmental Science and Technology* 42: 8858–8864.

Patterson WA, Edwards KJ, Maguire DJ (1987) Microscopic charcoal as a fossil indicator of fire. *Quaternary Science Reviews* 6: 3-23.

Payne RJ, Creevy A, Malysheva E, Ratcliffe J, Andersen R, Tsyganov AN, Rowson JG, Marcisz K, Zielińska M, Lamentowicz M, Lapshina E, Mazei Y (2016) Tree encroachment may lead to functionally-significant changes in peatland testate amoeba communities. *Soil Biology and Biochemistry* 98: 18-21.

Pech P, Wojtuń B, Samecka-Cymerman A, Polechońska L, Kempers AJ (2022) Metals in Plant Functional Types of Ombrotrophic Peatlands in the Sudetes (SW Poland). *Archives of Environmental Contamination and Toxicology* 82: 506–519.

Popowski B (2005) Results of a palynological analysis of peat sediments from Izerskie Bagno (Izerskie Mts). *Acta Botanica Silesiaca* 2: 95-106.

Quinto F, Hrnecek E, Krachler M, Shotyk W, Steier P Winkler SR (2013) Determination of ^{239}Pu, ^{240}Pu, ^{241}Pu ^{242}Pu at femtogram and attogram levels–evidence for the migration of fallout plutonium in an ombrotrophic peat bog profile. *Environmental Science: Processes & Impacts* 15(4): 839-847.

Ramsey CB (2009) Bayesian Analysis of Radiocarbon Dates. *Radiocarbon* 51(1): 337-360.

Rangwala I, Miller J (2012) Climate change in mountains: a review of elevation-dependent warming and its possible causes. *Climatic Change* 114: 527-547.

Reimer PJ, Brown TA, Reimer RW (2004) Discussion: Reporting and calibration of post-bomb C-14 data. *Radiocarbon* 46(3): 1299-1304.

Rose NL (2015) Spheroidal carbonaceous fly ash particles provide a globally synchronous stratigraphic marker for the Anthropocene. *Environmental Science and Technology* 49(7): 4155-4162.

Rosén K, Vinichuk M, Johanson K J (2009) ^{137}Cs in a raised bog in central Sweden. *Journal of Environmental Radioactivity* 100(7): 534-539.Rosnitschek-Schimmel I (1983) Biomass and Nitrogen Partitioning in a Perennial and an Annual Nitrophilic Species of Urtica. *Zeitschrift für Pflanzenphysiologie*109(3): 215-225.

Schell WR, Tobin MJ, Massey CD (1989) Evaluation of trace metal deposition history and potential element mobility in selected cores from peat and wetland ecosystems. *Science of the total environment* 87: 19-42.

Schönborn W (1965) Untersuchungen über die Zoochlorellen-Symbiose der Hochmoor-Testaceen. *Limnologica* (Berlin) 3: 173-176.

Segnana M, Oeggl K, Poto L, Gabrieli J, Festi D, Kofler W, Cesco Frare P, Zaccone C, Barbante C. (2020) Holocene vegetation history and human impact in the eastern Italian Alps: a multi-proxy study on the Coltrondo peat bog Comelico Superiore Italy. *Vegetation History and Archaeobotany* 29: 407–426.

Shotyk W (1988) Review of the inorganic geochemistry of peats and peatland waters. *Earth-Science Reviews* 25 (2): 95-176.

Shotyk W, Le Roux G (2005) Biogeochemistry and Cycling of Lead In: Sigel A et al (Ed. Dekker M) Biogeochemical Cycles of the Elements. *Metal Ions in Biological Systems* 43: 240-275.

Shotyk W, Cheburkin AK, Appleby PG, Fankhauser A, Kramers JD (1998) Lead in three peat bog profiles Jura Mountains Switzerland: enrichment factors isotopic composition and chronology of atmospheric deposition *Water, Air, and Soil Pollution* 100 (3–4): 297-310.

Shotyk W, Goodsite ME, Roos-Barraclough F, Heinemeier J, Frei R, Asmund G, Lohse C, Stroyer TH (2003) Anthropogenic contributions to atmospheric Hg, Pb, and As deposition recorded by peat cores from Greenland and Denmark dated using the ^{14}C AMS "bomb pulse curve". *Geochimica et Cosmochimica Acta* 67: 3991-4011.

Shotyk W, Weiss D, Kramers JD, Frei R, Cheburkin AK, Gloor M, Reese S (2001) Geochemistry of the peat bog at Etang de la Gru la Jura Mountains Switzerland and its record of atmospheric Pb and lithogenic trace metals (Sc Ti Y Zr and REE) since 12370 ^{14}C yr BP. *Geochimica et Cosmochimica Acta* 65: 14 2337–2360.

Skrzypek G, Baranowska-Kacka A, Keller-Sikora A, Jedrysek M-O (2009) Analogous trends in pollen percentages and carbon stable isotope composition of Holocene peat -

Possible interpretation for palaeoclimate studies. *Review of Palaeobotany and Palynology* 156(3-4): 507-518.

Smieja-Król B, Fiałkiewicz-Kozieł B (2014) Quantitative determination of minerals and anthropogenic particles in some Polish peat occurrences using a novel SEM point - counting method. *Environmental Monitoring and Assessment* 186: 2573-2587.

Smieja-Król B, Fiałkiewicz-Kozieł B, Michalska A, Krzykawski T, Smołka-Danielowska D (2019) Deposition of mullite in peatlands of southern Poland: Implications for recording large-scale industrial processes. *Environmental Pollution* 250: 717-727.

Smieja-Król B, Fiałkiewicz-Kozieł B, Sikorski J, Palowski B (2010) Heavy metal behaviour in peat - A mineralogical perspective. *Science of The Total Environment* 408 (23): 5924–5931.

Sobik M, Błaś M, Migała M, Godek M, Nasiółkowski T (2014) Klimat In: Knapik R Raj A (eds) Przyroda Karkonoskiego Parku Narodowego Karkonoski Park Narodowy Jelenia Góra DIMOGRAF Bielsko-Biała pp. 147–186.

Speranza A, Hanke J, Geel B, van Fanta J (2000) Late-Holocene human impact and peat development in the Cerná Hora bog Krkonose Mountains Czech Republic. *The Holocene* 10: 575-585.

Steinnes E, Friedland AJ (2006) Metal contamination of natural surface soils from long-range atmospheric transport: Existing and missing knowledge. *Environmental Reviews* 14(3): 169-186.

Storkey J, Stratonovitch P, Chapman DS, Vidotto F, Semenov MA (2014) A Process-Based Approach to Predicting the Effect of Climate Change on the Distribution of an Invasive Allergenic Plant in Europe. *PLoS ONE* 101371.

Strzyszcz Z, Magiera T (2001) Record of industrial pollution in Polish ombrotrophic peat bogs. *Physics and Chemistry of the Earth Part A: Solid Earth and Geodesy* 26(11-12) 859-866.

Swindles GT (2015) Spheroidal carbonaceous particles are a defining stratigraphic marker for the Anthropocene. *Scientific Reports* 5: 10264.

Swindles GT, Morris PJ, Mullan DJ, Payne RJ, Roland TP, Amesbury MJ, Lamentowicz M, Turner TE, Gallego-Sala A, Sim T, Barr ID, Blaauw M, Blundell A, Chambers FM,Charman DJ, Feurdean A, Galloway JM, Gałka M, Green SM, Kajukało K, Karofeld E, Korhola A, Lamentowicz Ł, Langdon P, Marcisz K, Mauquoy D, Mazei YA, McKeown MM, Mitchell EAD, Novenko E, Plunkett G, Roe HM, Schoning K, Sillasoo Ü, Tsyganov AN, van der Linden M, Väliranta M, Warner B (2019) Widespread drying of European peatlands in recent centuries. *Nature Geoscience* 12: 922-928.

Synal HA, Stocker M Suter M (2007) MICADAS: A new compact radiocarbon AMS system. *Nuclear Instruments & Methods in Physics Research Section B-Beam Interactions with Materials and Atoms* 259(1): 7-13.

Testa C, Jia G, Degetto S, Desideri D, Guerra F, Meli M A, Roselli C (1999) Vertical profiles of $^{239+240}$ Pu and ^{241}Am in two sphagnum mosses of Italian peat. *Science of the total environment* 232(1-2) 27-31.

Turetsky MR, Kotowska A, Bubier J, Dise NB, Crill P, Hornibrook ER, Minkkinen K, Moore TR, Myers-Smith IH, Nykänen H, Olefeldt D (2014) A synthesis of methane emissions from 71 northern temperate and subtropical wetlands. *Global Change Biology* 20(7): 2183–2197.

UNSCEAR 2000 Exposure from man-made sources of radiation Report volume 1: sources annex C.

Urban NR, Eisenreich SJ, Grigal DF, Schurr KT (1990) Mobility and diagenesis of Pb and ^{210}Pb in peat. *Geochimica et Cosmochimica Acta* 54(12): 3329-3346.

Urban G, Tomczyński K (2017) Air temperature trends at Mount Śnieżka (Polish Sudetes) and solar activity, 1881–2012. *Acta geographica Slovenica* 57(2):33-44.

Valde-Novak P (1999) Początki osadnictwa w Sudetach Instytut Archeologii i Etnologii PAN Kraków pp 238 (In Polish with English summary).

van Bellen S, Magnan G, Davies L, Froese D, Mullan-Boudreau G, Zaccone C, Garneau M, Shotyk W (2018) Testate amoeba records indicate regional 20th-century lowering of water tables in ombrotrophic peatlands in central-northern Alberta, Canada. *Global Change Biology* 24: 2758-2774.

van Bellen S, Mauquoy D, Hughes PD, Roland TP, Daley TJ, Loader NJ, Street-Perrott FA, Rice EM, Pancotto VA, Payne RJ (2016) Late-Holocene climate dynamics recorded in the peat bogs of Tierra del Fuego South America. *The Holocene* 26: 489-501.

van der Plicht J, Yeloff D, van der Linden M, van Geel B, Brain S, Chambers F M, Toms P (2013) Dating recent peat accumulation in European ombrotrophic bogs Radiocarbon 55(3): 1763-1778.

Vassilev SV, Greta M, Eskenazy GM, Vassileva CG (2001) Behaviour of elements and minerals during preparation and combustion of the Pernik coal Bulgaria. *Fuel Processing Technology* 72: 103–129.

Wardenaar EPC (1987) A new hand tool for cutting peat profiles. *Canadian Journal of Botany* 65: 1772-1773.

Waters CN, Syvitski JPM, Gałuszka A (2015) Can nuclear weapons fallout mark the beginning of the Anthropocene Epoch? *Bulletin of the Atomic Scientists* 71(3): 46–57.

Waters CN, Zalasiewicz J, Summerhayes C, Barnosky AD, Poirier C, Gałuszka A, Cearreta A, Edgeworth M, Ellis EC, Ellis M, Jeandel C, Leinfelder R, McNeill JR, Richter D, de B Steffen W, Syvitski J, Vidas D, Wagreich M, Williams M, Zhisheng An, Grinevald J, Odada E, Oreskes N, Wolfe AP (2016) The Anthropocene is functionally and stratigraphically distinct from the Holocene. *Science* 351: 137.

Waters CN, Zalasiewicz J, Summerhayes C, Fairchild IJ, Rose N, Loader NJ, Shotyk W, Cearreta A, Head MJ, Syvitski JPM, Williams M, Wagreich M, Barnosky AD, Zhisheng

A, Leinfelder R, Jeandel C, Gałuszka A, IvardoSul JA, Gradstein F, Steffen W, McNeill JR, Wing S, Poirier C, Edgeworth M (2018) Global Boundary Stratotype Section and Point (GSSP) for the Anthropocene series: Where and how to look for potential candidates. *Earth-Science Reviews* 178: 379-429.

Waters CN, Turner SD, Zalasiewicz J, Head MJ (2022, submitted) Candidate sites and other reference sections for the Global boundary Stratotype Section and Point (GSSP) of the Anthropocene series. *The Anthropocene Review.*

Wojtuń B (2006) Peat mosses (Sphagnaceae) in mires of the Sudetes Mountains (SW Poland): a floristic and ecological study. University of Agriculture, Wrocław- Poznan, pp. 225.

Wojtuń B, Samecka-Cymerman A, Kolon K, Kempers AJ (2018) Metals in *Racomitrium lanuginosum* from Arctic (SW Spitsbergen Svalbard archipelago) and alpine (Karkonosze SW Poland) tundra. *Environmental Science and Pollution Research* 25:12444–12450.

Woźniak Z (1970) Osadnictwo celtyckie w Polsce. Ossolineum, Wrocław (in Polish).

Xu J, Morris P J, Liu J, Holden J (2018) PEATMAP: refining estimates of global peatland distribution based on a meta-analysis. *Catena* 160: 134–140.

Yu ZC (2012) Northern peatland carbon stocks and dynamics: A review.*Biogeosciences* 9(10):4071-4085.

Zaccone C, Cocozza C, Cheburkin AK, Shotyk W, Miano TM (2007) Enrichment and depletion of major and trace elements, and radionuclides in ombrotrophic raw peat and corresponding humic acids. *Geoderma* 141(3-4): 235-246.

Zuna M, Mihaljevič M, Šebek O, Ettler V, Handley M, Navrátil T, Goliáš V (2011) Recent lead deposition trends in the Czech Republic as recorded by peat bogs and tree rings. *Atmospheric Environment* 45 (28): 4950-4958.

/

Fig.1. Map of the study site. The wind rose after Sobik (2014).

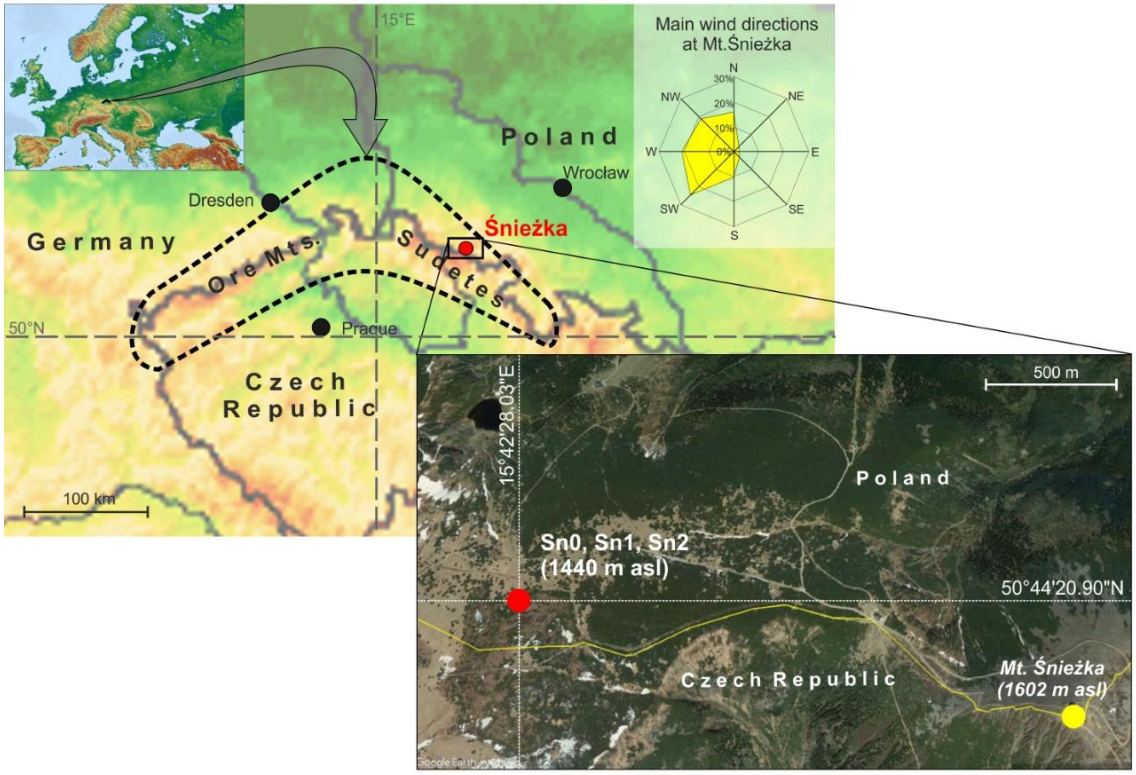

Fig.2. Results of macrofossil analysis and physical properties of all investigated cores.

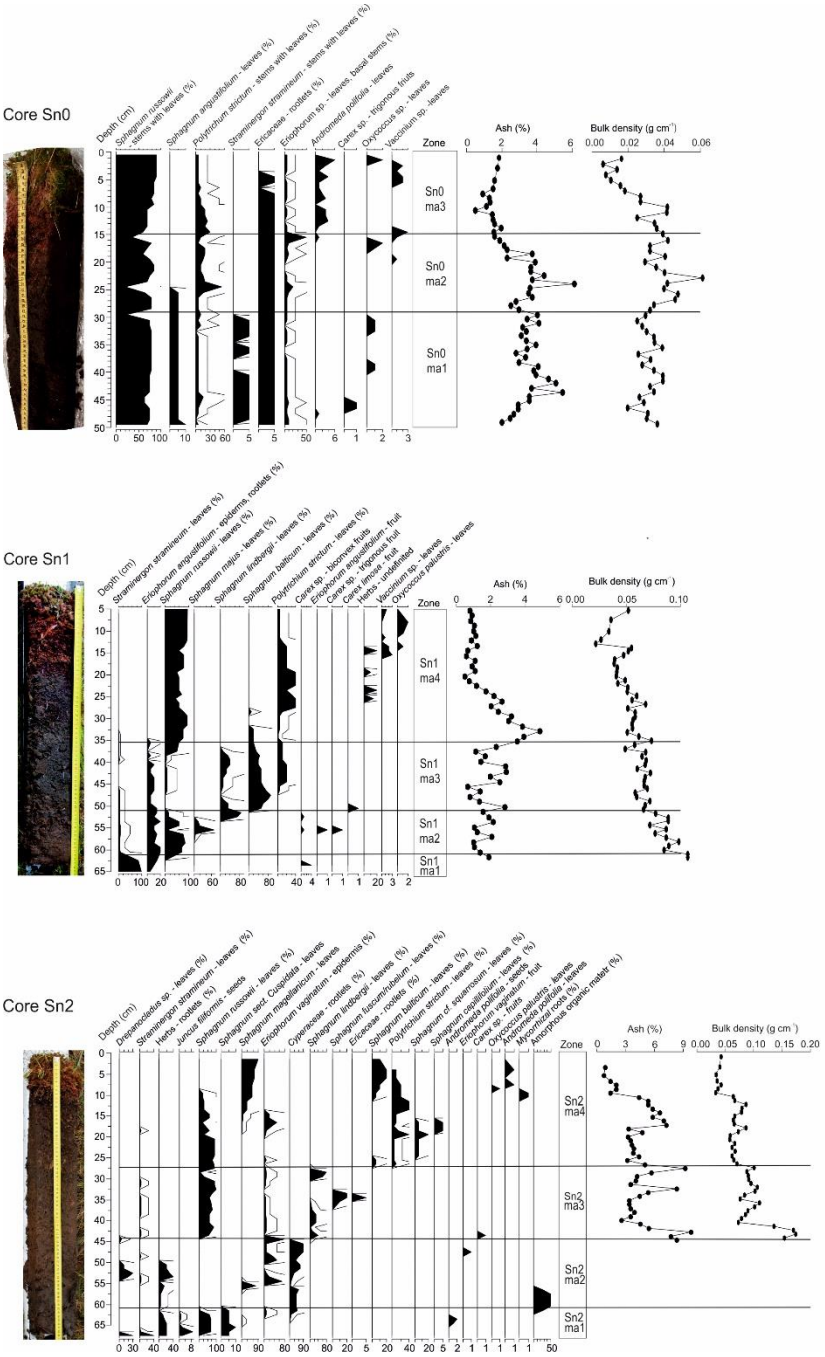

Fig.3. Comparison of $^{239+240}$Pu and ^{137}Cs vs. CF/CS modelled dates in Sn0 and Sn1.

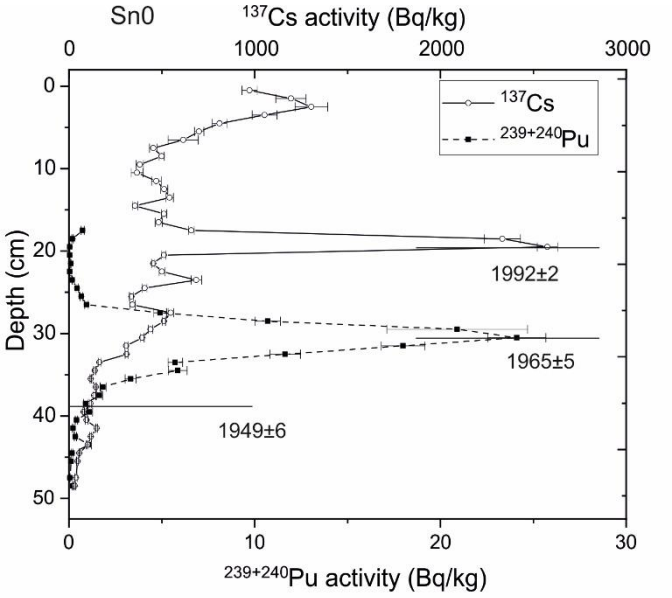

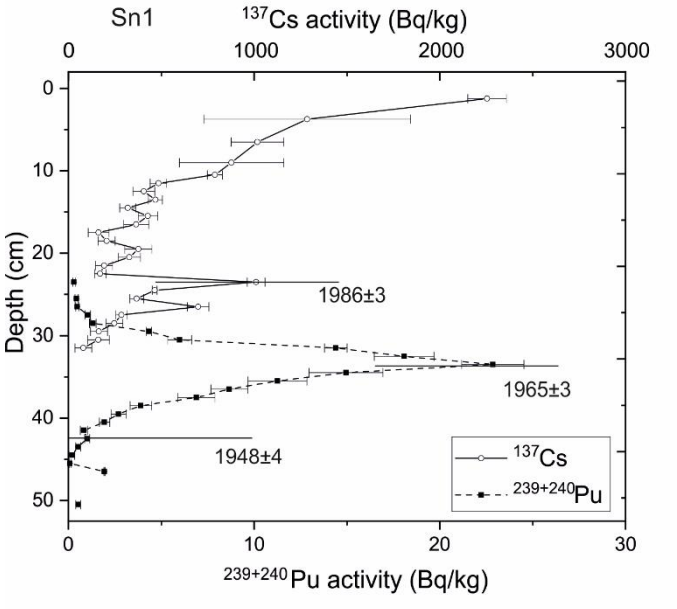

Fig.4. Geochemistry of Sn1 and Sn2 (based on Fiałkiewicz-Kozieł et al., 2020 except for mullite and sulphur). Sn1 profile records the appearance of 1952-Pu and spheroidal aluminosilicates (SAP) signal, while Sn2 SAP signal only, because of lack of measurements. The chronology is based on the $^{14}C/^{210}Pb$ model. At the depth of 41.5 cm (Sn1), the date of the first Pu appearance is provided, not measured in Sn2.

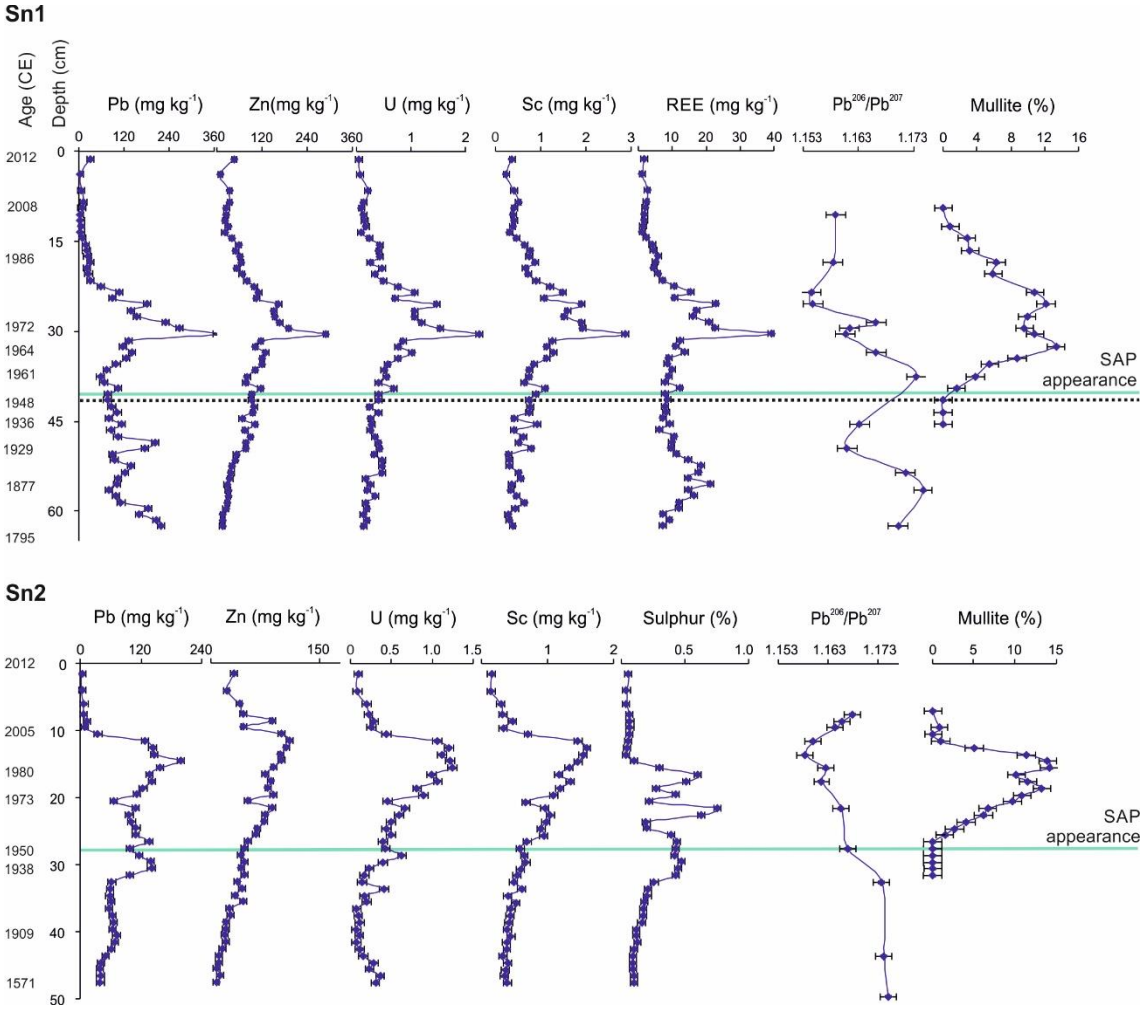

Fig.5. Simplified pollen diagram for Sn1 profile. 10 x exaggeration provided for better visualisation. At the depth of 41.5 cm, the date of the first Pu appearance is provided.

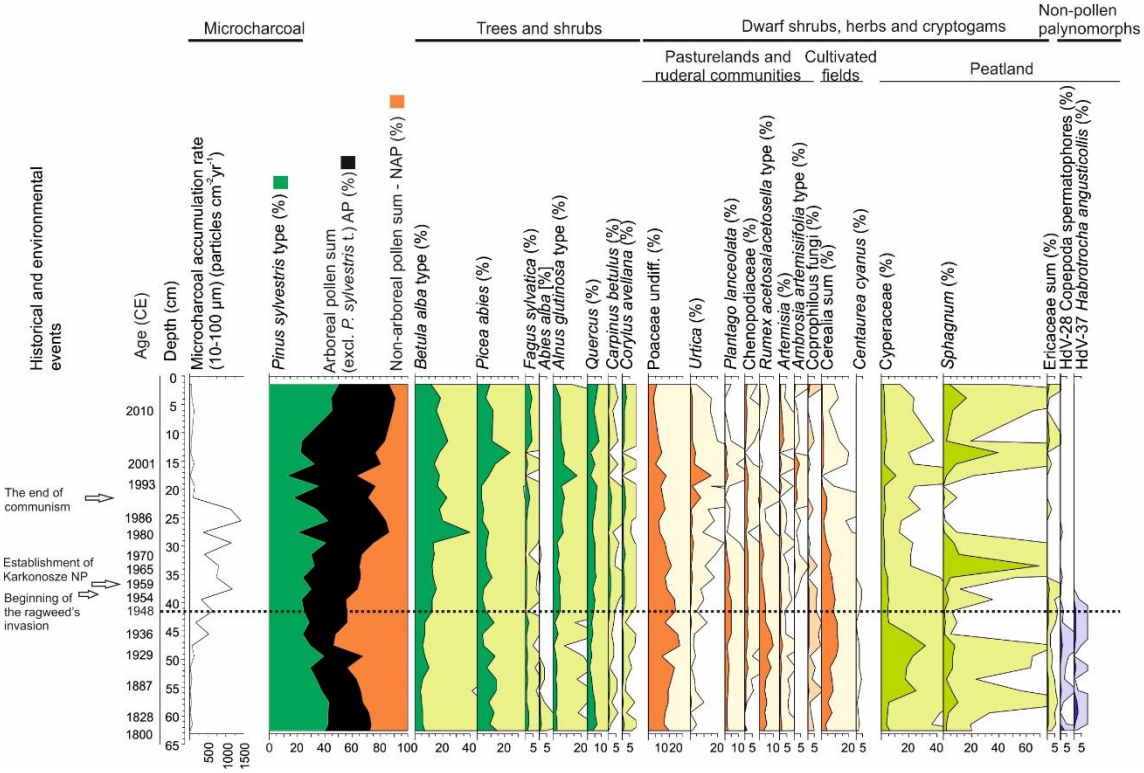

Fig.6. Short percentage diagram of the most frequent testate amoebae and reconstructed depth to the water table in Sn1 profile. In green - mixotrophs, orange – indicators of dry conditions. 5 x exaggeration provided for better visualisation. At the depth of 41.5 cm, the date of the first Pu appearance is provided.

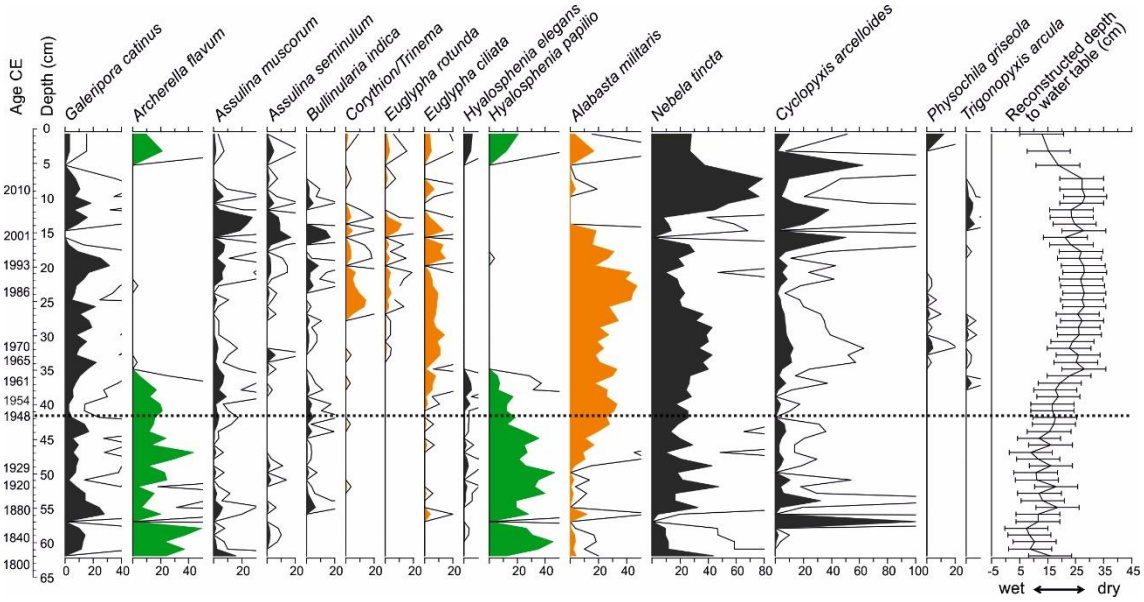

Fig.7. Summary of the most significant markers in Sn1. The horizontal dashed line is referred to first global Pu fallout (1952).

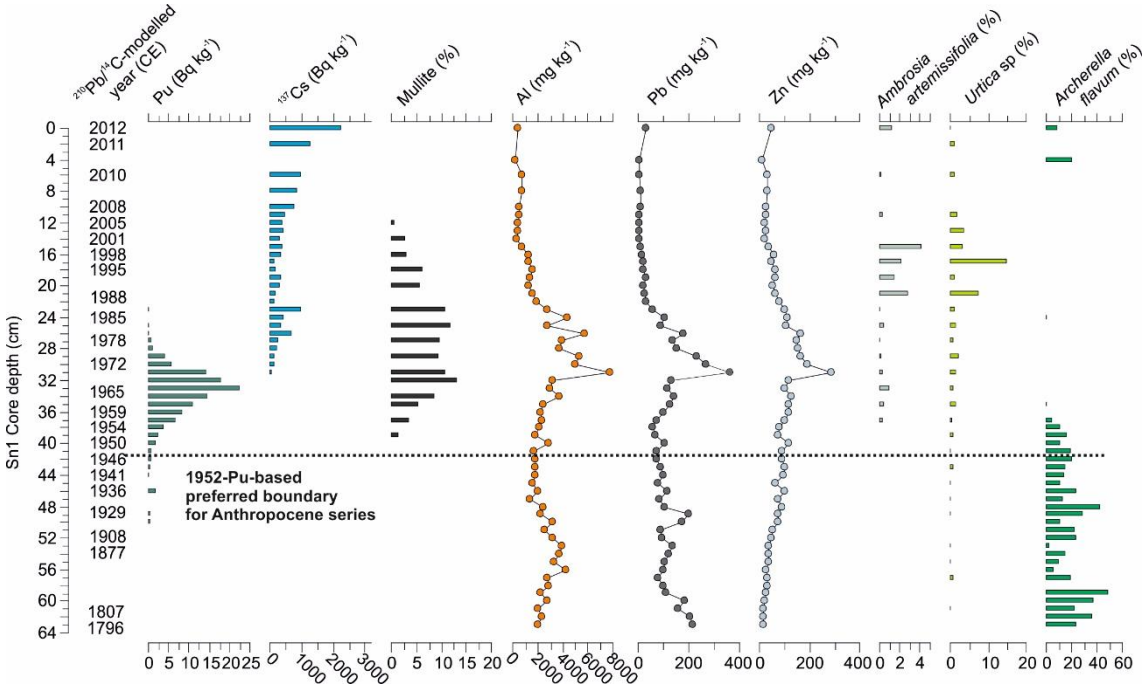

Fig.8. Summary of markers in Sn0. The horizontal dashed line is referred to first global Pu fallout (1952).

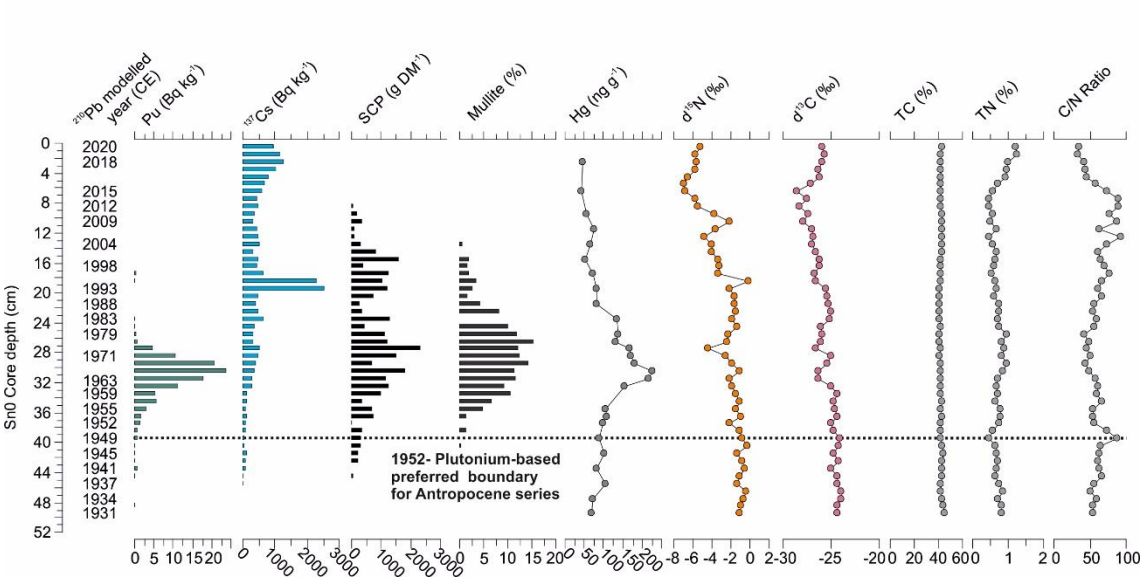

Fig.9. Non-metric multidimensional scaling (NMDS) diagrams for Śnieżka multiproxy dataset. NMDS shows a low-stress value (0.106) for the two-dimensional solution. Reconstructed depth to the water table (DWT) and geochemical data are projected on the ordination space. Codes for pollen types follow the pollen diagram (Fig. 5). Testate amoebae are projected as a sum of mixotrophic species ("TA Mixotrophs") and a sum of heterotrophic species ("TA Heterotrophs").

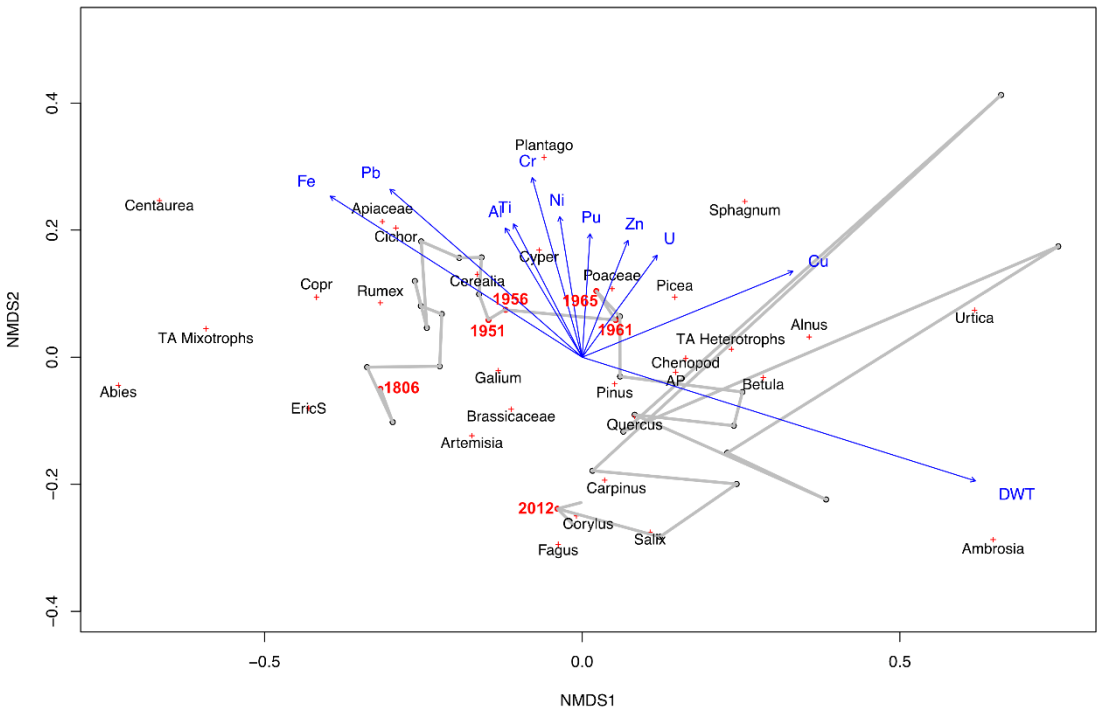

Fig.10. The comparison of $F^{14}C$ values (Sn0) (against ^{14}C age-depth model) with atmospheric curve and with Pu, which is presented against ^{210}Pb model. The overall similarity revealed between two independent models has confirmed the accuracy and robustness of both methods of dating.

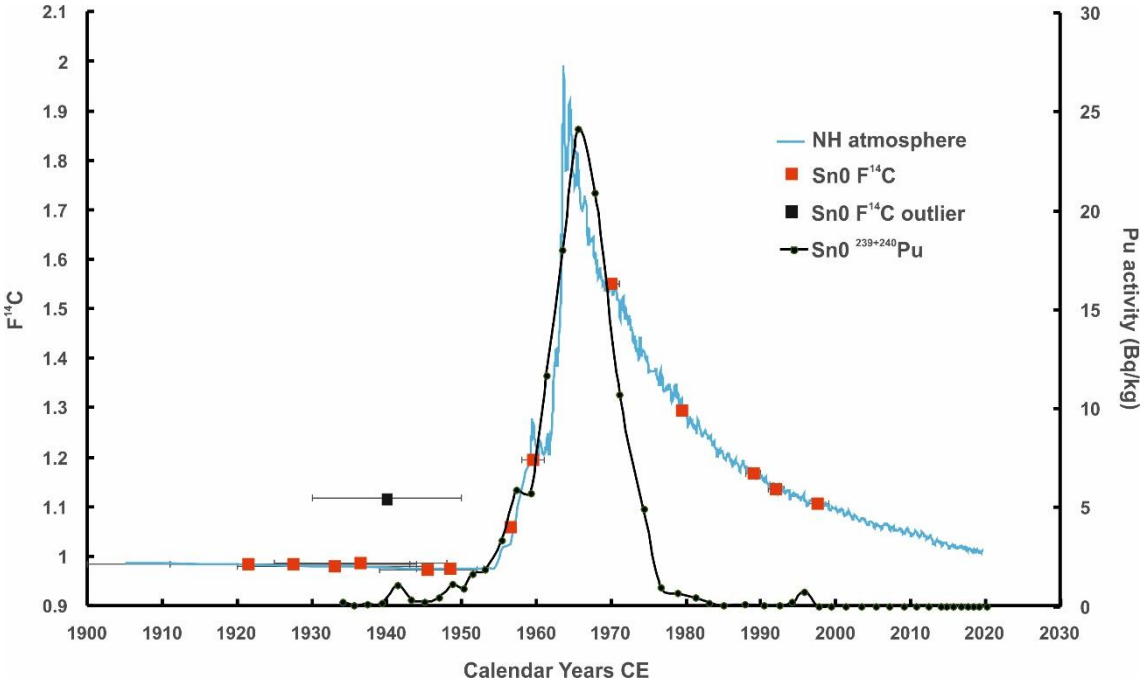

Fig.11.Fossil shell of a testate amoeba from the depth 25-26 cm with fly ash (red circles) built in the shell.

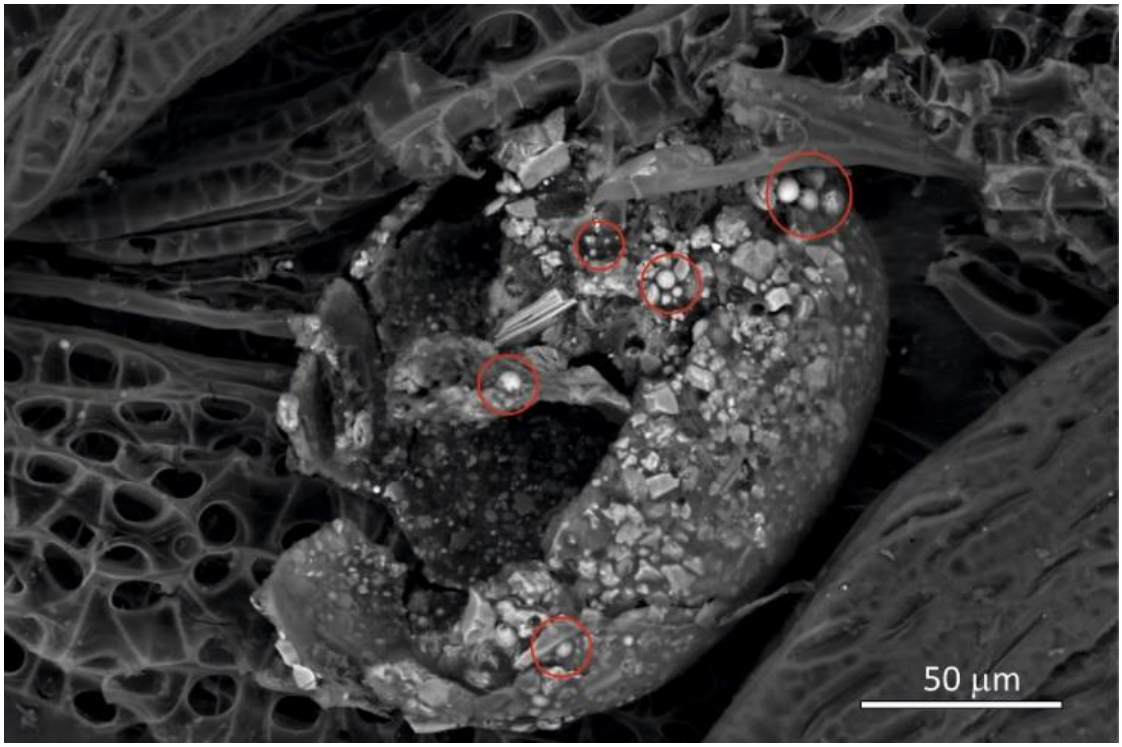

Supplementary material 1

2.3 Methods

2.3.1 Macrofossils and physical properties. The basic physical properties of the peat profiles (Sn1, Sn2, Sn0) were analysed in every slice (1cm) using standard procedures (Fiałkiewicz-Kozieł et al., 2020). High-resolution (1-cm peat slices) plant macrofossil analysis was used to reconstruct local ecological conditions and peat-forming plants in contiguous samples of approximately 20 cm^3 in all profiles (comp. Suppl.1). Macrofossil samples were washed and sieved through a 0.2-mm mesh. Peat composition was determined based on carpological remains and vegetative fragments (leaves, rootlets, epidermis) using the available identification keys (e.g. Mauquoy and van Geel, 2007). The identification of *Sphagnum* to species level was carried out separately on stem leaves using specific keys (Hölzer, 2010).

2.3.2 Chronological controls the chronology of Sn0 was obtained using ^{210}Pb, measured in every slice, and compared to ^{137}Cs and $^{238,239+240}$Pu chronomarkers as well as to F^{14}C. ^{14}C was assessed for Sn1 and Sn2, while artificial radionuclides and ^{210}Pb were established for Sn1.

^{238}Pu, ^{239,240}Pu Activities of ^{238}Pu, ^{239,240}Pu were determined on 0.08–0.88 g of dried sample (for Sn1 and Sn0). Chemical recoveries were determined using ^{242}Pu ($T_{1/2}$ = 373

300 y) as a yield tracer. Samples were leached with a boiling mixture of HNO_3, HCl and H_3BO_3. The solution was converted to 1M HNO_3. The next step was adjusting the Pu oxidation state to +4 using hydrazine hydrate, $NaNO_2$ and HNO_3. The final feed solution of 8M HNO_3 passed through the column filled with Dowex 1x8 anion-exchange resin in nitric form. Pu was stripped with 0.1M HF and 0.1M HCl after eluting thorium with 10M HCl (Łokas et al., 2010; Cwanek et al., 2021). Pu alpha sources were prepared by the NdF_3 co-precipitation method (Sill, 1987). The chemical recoveries averaged 68 ± 4% and 97 ± 4% (±SD, 1σ) for Pu isotopes. Measurements of $^{238,\ 239+240}$Pu activities were carried out using an alpha-particle spectrometer (Alpa Analyst, Canberra) with semiconductor, passivated planar silicon detectors (PIPS, Canberra). The blank analysis did not exhibit any experimental biases. Reference material IAEA 447 was processed together with research material to ensure the quality and accuracy of the undertaken analysis. The results corresponded well with the certified values.

^{210}Pb, ^{137}Cs Activities of ^{210}Pb, ^{137}Cs were determined for each sub-sample of Sn0 through gamma-ray spectrometry using a high purity germanium detector (DSG, Germany) located at the Institute of Physics Jagiellonian University. ^{210}Pb and ^{137}Cs were determined using its gamma emission (Eγ = 46.5keV and 661.6 keV). The detector was built from a n-type, coaxial germanium crystal with thin p+ contact ensuring high detection efficiency for low-energy gamma and x-rays. The relative efficiency of the

detector is 60 percent compared to the standard, 3x3 inch NaI (Tl) scintillator and the measured energy resolution is 2.1 keV at a 1332 keV line emitted by ^{60}Co. Germanium crystal is closed in a low background endcap with thin aluminium window and additionally shielded by placing lead layer above J-Fet and feedback resistor. The detector is placed in a low activity (>6 Bqkg^{-1}) lead shield constantly flushed with gaseous nitrogen boiling off from dewar. Passive shielding is also surrounded by five EJ-200 scintillators and borated polyethylene panels. Standard NIM electronics process signals from HPGe and veto detectors and spectra were collected by MCA4 software (FastCommTech). After the acquisition, spectra were stored in ASCII format and analysed using Tukan 8K software (NCBJ, Poland). Efficiency calibration of the detector was simulated using GEANT4 software and validated by counting standard reference materials IAEA-410 and IAEA-447.

Fresh, wet samples intended for gamma-ray spectrometry were placed in the small Petri dishes (diameter 5.0 cm, height 1.6 cm) wiped with isopropanol and placed on top of the detector end cap. After measurement, samples were taken back to the Institute of Nuclear Physics PAS, dried at 105º C and weighted to determine the dry mass used in specific activities calculation.

^{210}Pb was analysed by alpha spectrometry in the Sn1 profile (Fiałkiewicz-Kozieł et al., 2020). The activity of a total ^{210}Pb was determined indirectly by measuring its decay product, ^{210}Po, using alpha spectrometry. ^{210}Po was chemically extracted from the

material. Po isotopes were deposited on an Ag disc. Solution after polonium separation was used for Pu separation. Activity concentrations for polonium isotopes were determined using alpha spectrometers (Ortec Alpha Duo with Ortec ion-implanted silicon detectors).

The supported level ($^{210}Pb_{sup}$) was obtained as the mean value (±SD, 1σ) of activities for the lowermost layers, where the level of $^{210}Pb_{tot}$ has reached a steady state. By subtracting $^{210}Pb_{sup}$ activity from $^{210}Pb_{tot}$ activity on a level-by-level basis, the unsupported fraction ($^{210}Pb_{uns}$) was calculated. Annual accumulation rates (SAR, gcm^{-2} yr^{-1}) were calculated from peat bulk density and the thickness of individual slices. The cumulative mass depth (gcm^{-2}) was calculated by summing up annual accumulation rates.

The CF/CS model was applied in the profiles Sn1 and Sn0. The Constant Flux Constant Sedimentation model (CF/CS; Sanchez-Cabeza and Ruiz-Fernández, 2012) allowed calculations of the peat ages at different depth intervals. This model assumes a constant atmospheric flux of ^{210}Pb to the peat surface and a continuous peat accumulation rate. the age modelled was assigned to a depth mid-point of each sample.

^{14}C Fourteen samples of macrofossils from core Sn0 were analyzed at the AMS facility ETH Zurich. Samples underwent the Acid-Base-Acid treatment (Hajdas 2008), were graphitized (Nemec et al., 2010), and analyzed using the MICADAS system (Synal et al., 2007). It was impossible to create the combined model using ^{210}Pb and ^{14}C, because we sampled material for dating one month after first sampling and we noticed some extending

of peat profile. However, we were able to create age-depth model based on ^{14}C and plotted it with atmospheric curve. Then we compared two obtained models – CF/CS model with our $F^{14}C$ data and NH1 curve (Hua et al., 2021) The overall similarity revealed between two independent models has confirmed the accuracy and robustness of both methods of dating.

Hand-picked plant macrofossils, stored in MilliQ water, were selected for ^{14}C dating of Sn1 and Sn2. Seven samples from Sn1 and five samples from Sn2 were measured at the Radiocarbon Laboratory in Poznań, Poland. An absolute chronology was based on the age-depth model published by Fiałkiewicz-Kozieł et al. (2020) and recalculated with the application of the IntCal20 (Reimer et al., 2020) atmospheric curve. The differences between the new model and the one published by Fiałkiewicz-Kozieł et al. (2020) were negligible.

For better readability, the modelled dates were expressed as μ (mean) values of modelled ranges of age, expressed as CE (=Common Era) in the following sections of the text.

2.3.3 Pb, Zn, Cu, Ni, Cr, Sr, Ti, Al, and REE concentrations Peat samples were dried at 105ºC before ashing at 550ºC and a two-step acid digestion in Teflon Savillex® beakers. Residue after combustion at 550◦C was referred to as ash content. First, samples were treated with 4,5 ml of suprapure 65% HNO_3 and 0,5 ml of 45% HF for 48h at 130ºC. They were then evaporated and treated with 1 ml of concentrated HCl for 24 h in 90 ºC.

After final evaporation, residues were diluted in 10 % HNO_3 and measured using ICP-MS at the UAM for trace metals and *Observatoire Midi-Pyrénées* (Toulouse, France) for Rare Earth Elements. All measurements were performed in duplicate. NIMT (peat, Yafa et al., 2004) and CTA-OTL-1 (tobacco leaves) certified reference materials were used to monitor the accuracy of measurements. Certified value of NIMT equals: Al - 3692 ± 347 mg kg^{-1}; Cr - 6.36 ± 0.44 mg kg^{-1}; Cu - 5.28 ± 1.04 mg kg^{-1}; Fe - 921 ± 84 mg kg^{-1}; Pb - 174 ± 8 mg kg^{-1}; Ti - 357 ± 18 mg kg^{-1}; Zn - 28.6 ± 1.9 mg kg^{-1}, La -1.24 ± 0.03 mg kg^{-1}, Sm – 0.194 ± 0.005 mg kg^{-1}. Measured CRM values fall within 97 % of the certified values for Al, Ti, Cr, Cu, Fe, Pb, Zn, and 85-86% for La and Sm. The analytical deviation is less than 5%.

2.3.4 Hg (Sn0) Total mercury concentrations were measured at UCL Geography. Twenty-seven freeze-dried peat core samples from Sn0 were digested with 7 ml *aqua regia* ($HCl+HNO_3$) at 100°C on a hotplate for 2h in rigorously acid-leached 50 ml polypropylene digestion tubes. Standard reference material stream sediment GBW07305 (certified Hg value is 100 ± 10 ng g^{-1}; and measured mean value is 103.2 ng g^{-1}, with SD = 8.3 ng g^{-1} (n=2). Sample blanks were digested with the samples. Digested solutions were analysed for Hg using cold vapour-atomic fluorescence spectrometry (CV-AFS) following reduction with $SnCl_2$. Standard solutions and quality control blanks were measured in every five samples to monitor measurement stability.

2.3.5 Pb isotopes Ten to 500 mg of dry peat and rocks powder was taken to obtain 2000 ng of Pb in the final solution. The sample powders were ashed (550°C, 4h) prior to digestion in 6 ml HF *suprapur* (Merck) + 1 ml HNO_3 65% *cc. sub.* in Teflon beakers (120°C, 48h) in class 1000 clean room (UAM, Poznań). Dried residues were dissolved in HBr 6% *cc. sub.* before chromatographic separation. Lead was separated using anionic exchange micro-columns (Weis et al., 2005) and sub-boiled distilled acids. The measurements were conducted on TIMS Finnigan MAT-261 special (UAM). The instrumental drift was controlled by standard bracketing using NBS981 standard data (Galer and Abouchami, 1998). Repeated standard measurements for NBS981 equal: $^{208/204}Pb = 36.756 \pm 0.013$, $^{207/204}Pb = 15.484 \pm 0.018$ and $^{206/204}Pb = 16.937 \pm 0.010$ and are comparable with recommended values: $^{206}Pb/^{204}Pb = 16.9406 \pm 0.0003$; $^{207}Pb/^{204}Pb = 15.4957 \pm 0.0002$, $^{208}Pb/^{204}Pb = 36.7184 \pm 0.0007$ (Taylor et al., 2015).

2.3.6 Carbon, Nitrogen and Sulfur (Sn2) Total nitrogen (N), carbon (C), and sulphur (S) values were determined in dried and homogenized samples with a VarioMax CNS elemental analyzer (Elementar Analyzensysteme GmbH, Germany). Owing to the absence of carbonates, total carbon was presumed equal to total organic carbon (TOC). The TOC/N ratio was calculated on a molar basis. The analytical quality was assessed via duplicate measurements of the samples as well as by the use of certified reference

materials (Sulfadiazine and Peaty soil by Elementar, Germany). The reproductivity of CRM values for C, N and S was >95%.

2.3.7 CN, C and N isotopes (Sn0) Samples were homogenised using a ball mill and 1mg of ground material was weighed into tin cups. Samples were analysed on an elemental analyser (ANCA GSL, Sercon, UK) and combusted over chromium (III) oxide at 1000°C and reduced over activated copper at 600°C, water was removed using a magnesium perchlorate scrubber. N_2 and CO_2 were separated using gas chromatography and subsequently isotopic ratios and quantifications were determined using an isotope ratio monitoring mass spectrometer (20-20MS, Sercon, UK). Certified reference materials, calibrated against IAEA-CH-6 and IAEA-N-1 (Elemental Microanalysis, Oakhampton, UK) were measured every 9 samples. A blank correction was applied to all nitrogen analysis. Total nitrogen (TN), total organic carbon (TOC) is expressed in mass as percentage values, C:N ratios were calculated on a mass basis and stable isotopic composition relative to the standards were expressed in per mill values according to the delta notation: $\delta X = [(R_{sample}/R_{standard}) - 1] \times 100$, where δX is $\delta^{13}C$ or $\delta^{15}N$, and R is the respective $^{13}C/^{12}C$ or $^{15}N/^{14}N$ ratio. (Nitrogen isotopes as δ15N vs air and carbon isotopes as $\delta^{13}C$ vs V-PDB). Precision and accuracy were 0.1 per mill for both $\delta^{15}N$ and $\delta^{13}C$.

2.3.8 Technofossils

Spheroidal Carbonaceous Particles (Sn0) Sn0 was analysed for SCPs following the method described in Rose (1994), repeating the nitric acid step to remove all organic-rich material. Dried sediment was subjected to sequential chemical digestion by mineral acids to remove unwanted fractions leaving a suspension of mainly carbonaceous material and a few persistent minerals in water. SCPs are composed mostly of elemental carbon and are chemically robust. The use of concentrated nitric acid (to remove organic material), hydrofluoric acid (siliceous material) and hydrochloric acid (carbonates and bicarbonates) therefore does them no damage. A known fraction of the final suspension was evaporated onto a coverslip and mounted onto a microscope slide. The number of SCPs on the coverslip was counted using a light microscope at x400 magnification and the concentration was calculated in units of 'a number of particles per gram dry mass of sediment' (gDM^{-1}). The criteria for SCP identification under the light microscope followed Rose (2008). The detection limit for the technique is typically c. 100 gDM-1 and concentrations have an accuracy of c. ± 45 gDM^{-1} (Rose 2008). However, detection limits were slightly lower in the upper 12 cm of this core (c. 50 gDM^{-1}). Analytical blanks were included in duplicate as well as SCP reference material (Rose, 2008). Reference concentrations agreed closely with expected values (6005 ± 70 gDM^{-1}), while no SCPs were observed in the blanks.

SAP and mullite (Sn0, Sn1, Sn2) The shape, size, morphology, and chemical composition of dust particles were determined in peat samples using the backscattered electron detector (BSE) of a scanning electron microscope (SEM) equipped with an energy-dispersive X-ray analysing system (SEM-FEI Quanta 250; University of Silesia in Katowice). The accelerating voltage was 15 kV and 10 mm the working distance. Air-dried peat samples were gently homogenised using a corundum mortar and pestle. A thin layer of each homogenised sample was fixed to a double-sided 9 mm carbon tab, placed on an aluminium stub, and carbon-coated prior to analysis.

Mullite content was determined in the profiles using x-ray diffraction (XRD), following the method described in Smieja-Król et al. (2019). For the XRD analysis, peat samples were ashed at 500°C and treated with 1 M HCl for 15 min to remove the acid-soluble ash fraction (Sapkota, 2006). The residue was dried, ground in an agate mortar, and analysed using a Panalytical X'Pert PRO PW 3040/60 X-ray diffractometer (University of Silesia in Katowice). The instrument was equipped with a Ni-filtered Cu Kα source radiation (λ = 1.540598 Å) and an X'Celerator strip detector. Samples were scanned within a 2Θ interval of 2.5-65°, with a step size of 0.01° 2Θ and a counting time of 300 s. Identification and quantification of mineral phases were done through the X'Pert HighScore Plus Software using the newest ICSD database. Quantitative contents were calculated using the Rietveld method. The detection limit of the XRD method was 0.5-1%, depending on the ash phase composition. Analytical precision and accuracy were ±3%.

2.3.9 Biostratigraphy

Pollen, non-pollen palynomorphs, microcharcoal (Sn1) Material for palynological analysis were taken from every second slice and a total of 30 samples were prepared using standard laboratory procedures (Berglund and Ralska-Jasiewiczowa, 1986). To remove the mineral fraction, samples were treated with 10% hydrochloric acid (to dissolve carbonates), heated in 10% potassium hydroxide (to remove humic compounds), and finally soaked in 40% hydrofluoric acid for 24 h (to remove the silicates), followed by acetolysis. Two *Lycopodium* tablets were added to each sample during the laboratory procedures to calculate microfossil concentration (Stockmarr, 1971). Pollen, spores, and selected non-pollen palynomorphs (NPPs) were counted under an upright microscope until the number of total pollen sum (TPS) grains in each sample reached at least 500 (except for 8 samples in which the pollen concentration was extremely low). Sporomorphs were identified with the assistance of atlases and keys (Moore et al., 1991; Beug, 2004; van Geel and Aptroot, 2006). Additionally, microscopic charcoal (fraction size: 10-100 μm) was counted on pollen slides.

Testate amoebae (Sn1) Testate amoebae were analysed continuously in sub-samples of 4 cm^3. Peat samples were washed under 250 μm sieves following the method described by Booth et al. (2010). The testate amoebae were analysed under the light microscope

with 250 and 400 magnifications, aiming at a minimum of 150 tests per sample (Booth et al., 2010). Several keys and taxonomic monographs (Grospietsch, 1958; Ogden and Hedley, 1980; Meisterfeld, 2001; Clarke, 2003; Mazei and Tsyganov, 2006) were used to achieve the highest taxonomic resolution.

The results are presented as percentages of the abundance of the total testate amoebae sum counted. Testate amoebae record has been used for the quantitative reconstruction of past water table depth. The water table was reconstructed using the European calibration data set (Amesbury et al., 2016), and hydrological dynamics closely follow the taxonomic changes along the profile.

2.3.10 Statistical methods The testate amoeba-based water table reconstruction (DWT) has been performed in the C2 software (Juggins, 2007) was reconstructed using the European calibration data set (Amesbury et al., 2016), and hydrological dynamics closely follow the taxonomic changes along the profile.

Non-metric multidimensional scaling (NMDS) was used to define the relationships between geochemical data, water table reconstruction and the response of testate amoeba and vegetation (pollen data) to anthropogenic forcing. NMDS was computed using Bray-Curtis distance measure, and the data undergone square root transformation and Wisconsin double standardization. NMDS was performed using the software R (R Development Core Team, 2014) and the package ‘vegan’ (Oksanen et al., 2017).

References

Amesbury MJ, Swindles GT, Bobrov A, Charman DJ, Lamentowicz M, Mallon G, Mazei Y, Mitchell EAD, Payne RJ, Roland TP, Turner ET, Warner BG (2016) Development of a new pan-European testate amoeba transfer function for reconstructing peatland palaeohydrology. *Quaternary Science Reviews* 152: 132-151.

Berglund BE and Ralska-Jasiewiczowa M (1986) Pollen analysis and pollen diagrams. In Berglund BE (ed) Handbook of Holocene Palaeoecology and Palaeohydrology. Chichester–New York–Brisbane–Toronto–Singapore: John Wiley & Sons, pp. 455–484.

Beug HJ (2004) Leitfaden der Pollenbestimmung für Mitteleuropa und angrenzende Gebiete. Verlag Dr. Friedrich Pfeil. München.

Booth RK, Lamentowicz M, Charman DJ (2010) Preparation and analysis of testate amoebae in peatland paleoenvironmental studies. *Mires and Peat* 7: 1-7.

Clarke KJ (2003) Guide to Identification of Soil Protozoa - Testate Amoebae. Freshwater Biological Association, Ambleside UK.

Fiałkiewicz – Kozieł B, Łokas E, Gałka M, Kołaczek P, De Vleeschouwer F, Le Roux G, Smieja-Król B (2020) Influence of transboundary transport of trace elements on mountain peat geochemistry (Sudetes Central Europe). *Quaternary Science Reviews* 230: 106162.

Grospietsch T (1958) Rhizopoden-Analyse der Moore. In: Moor SIpl (eds) VI

Internationalen Kongress für Universelle Moorforschung Brüssel und Spa, pp. 175-182.

Juggins S (2007) C2 Version 15 User guide Software for ecological and palaeoecological data analysis and visualisation. Newcastle University Newcastle upon Tyne UK, pp. 73.

Hajdas I (2008) The Radiocarbon dating method and its applications in Quaternary studies. *Quaternary Science Journal - Eiszeitalter und Gegenwart* 57(1/2):2-24.

Hölzer A (2010) Die Torfmoose Südwestdeutschlands und der Nachbargebiete. WeissdornVerlag Jena, Jena.

Łokas E, Mietelski JW, Kleszcz K, Tomankiewicz E (2010) A sequential procedure for determining ^{238}Pu, $^{239+240}$Pu, ^{241}Am, ^{90}Sr, U and Th activities in soils and peats from Spitsbergen. *Nukleonika* 55: 195-199.

Mauquoy D, van Geel B (2007) Mire and peat macros. In: *Encyclopedia of Quaternary Science. Elias* S.A. (ed.). pp. 2315-2336. Elsevier, Amsterdam.

Mazei Y, Tsyganov AN (2006) Freshwater testate amoebae, KMK Moscow.

Meisterfeld R (2001) Testate amoebae in: Costello MJ Emblow CS White R (Eds) Patrimoines Naturels Muséum National d'Histoire Naturelle - Institut d'Ecologie et de Gestion de la Biodiversité (IEGB) - Service du Patrimoine Naturel (SPN) Paris, pp. 54-57.

Moore PD, Webb JA and Collinson ME (1991) Pollen analysis. Blackwell Scientific Publications, Oxford.

Nemec M, Wacker L, Gaggeler H (2010) Optimization of the Graphitization Process at Age-1. *Radiocarbon* 52(3): 1380-1393.

Ogden CG, Hedley RH (1980) An Atlas of Freshwater Testate Amoebae, Oxford University Press London.

Oksanen J, Blanchet FG, Friendly M, Kindt R, Legendre P, McGlinn D, Minchin PR, O'Hara RB, Simpson GL, Solymos P, Stevens MHH, Szoecs E, Wagner H (2017) vegan: Community Ecology Package R package version 24-2.

R Development Core Team (2014) R: A Language and Environment for Statistical Computing Vienna: R Foundation for Statistical Computing.

Reimer PJ, Brown TA, Reimer RW (2004) Discussion: Reporting and calibration of post-bomb C-14 data. *Radiocarbon* 46(3): 1299-1304.

Reimer P, Austin W, Bard E, Bayliss A, Blackwell P, Bronk Ramsey C, Butzin M, Cheng H, Edwards R, Friedrich M, Grootes P, Guilderson T, Hajdas I, Heaton T, Hogg A, Hughen K, Kromer B, Manning S, Muscheler R, Palmer J, Pearson C, van der Plicht J, Reimer R, Richards D, Scott E, Southon J, Turney C, Wacker L, Adolphi F, Büntgen U, Capano M, Fahrni S, Fogtmann-Schulz A, Friedrich R, Köhler P, Kudsk S, Miyake F, Olsen J, Reinig F, Sakamoto M, Sookdeo A, Talamo S (2020). The IntCal20 Northern Hemisphere radiocarbon age calibration curve (0–55 cal kBP). *Radiocarbon* 62.

Sanchez-Cabeza JA, Ruiz-Fernández AC (2012) ^{210}Pb sediment radiochronology: an integrated formulation and classification of dating models. *Geochimica et Cosmochimica Acta* 82:183-200.

Sill, C.W. (1987) Precipitation of actinides as fluorides or hydroxides for high resolution alpha spectrometry. Nucl. Chem. *Waste Management* 7, 201–215.

Stockmarr J (1971) Tablets with spores used in absolute pollen analysis. *Pollen et Spores* 13: 615–621.

Synal HA, Stocker M Suter M (2007) MICADAS: A new compact radiocarbon AMS system. *Nuclear Instruments & Methods in Physics Research Section B-Beam Interactions with Materials and Atoms* 259(1): 7-13.

van Geel B and Aptroot A (2006) Fossil ascomycetes in Quaternary deposits. *Nova Hedwigia* 82: 313–329.

Yafa, C., Farmer, J.G., Graham, M.C., Bacon, J.R., Barbante, C., Cairns, W.R.L., Bindler, R., Renberg, I., Cheburkin, A., Emons, H., Handley, M.J., Norton, S.A., Krachler, M., Shotyk, W., Li, X.D., Martinez-Cortizas, A., Pulford, I.D., MacIver, V., Schweyer, J., Steinnes, E., Sjøbakk, T.E., Weiss, D., Dolgopolova, A. and Kylander, M. (2004) Development of an ombrotrophic peat bog (low ash) reference material for the determination of elemental concentrations. *Journal of Environmental Monitoring* 6, 493–501.

Supplementary material 2

Description of macrofossil zones The zones marked as "ma" represent the individual phases of the development of local plant succession at three sampling sites. Zones ma1-ma4 have been distinguished based on the presence of dominant species in the peat layers. The dominant species were also the main peat-forming species.

Three zones in local vegetation development were visually delimited in the macrofossil diagram of core Sn0 (Fig. 2). Zone Sn0-ma-1 (49.5-28.5 cm) was dominated by *S. russowii*, *S. angustifolium* and *S. stramineum*. In zone Sn0-ma-2 (28.5-12.5 cm) *S. russowii*, *P. strictum*, and *Eriophorum* sp. played a dominant role. The domination of *S. russowii* characterized the zone Sn0-ma-3 (13.5-0 cm). *Andromeda polifolia* leaves were also recorded in the latter zone.

Four zones in local vegetation development were visually delimited in the macrofossil diagrams of core Sn1 and Sn2 (Fig.2). In zone SnI-ma-1 (62.5-60.5 cm) *Straminergon stramineum* was a dominant species. During zone SnI-ma-2 (60.5-52.5 cm) *Sphagnum russowii* and *Eriophorum angustifolium* were dominant species. In zone Sn1-ma-3 (52.5-35.5 cm) *Sphagnum lindbergii* followed by *S. balticum* and *Polytrichum strictum* played a dominant role. Zone Sn1-ma-4 (35.5-0 cm) was characterized by domination *S. russowii* and *P. strictum*. *Oxyccocus palustris* and *Vaccinium* sp. leaves were recorded in the uppermost part of this zone. In zone Sn2-ma-1 (67-61 cm), *S. russowii* and *S.* sect.

Cuspidata were a dominant species. *Juncus filiformis* seeds were also found. In zone SnII-ma-2 (61-44 cm), *Eriophorum vaginatum*, Cyperaceae, and brown moss were mainly recorded. During zone Sn2-ma-3 (44-27 cm), *S. russowii* and *S. lindbergii* were dominant species, and there was a peak of *S. fuscum/rubellum*. Zone Sn2-ma-4 (27-0 cm) is dominated by *S. russowii* and *P. strictum* in the bottom part and *S. medium/divinum* and *S. balticum* in the upper part of this zone.

Supplementary table 1 Pu, Cs and ^{210}Pb activities as well as dates derived from CF/CS model *(MDC*- minimum detectable activity*)*

Depth (cm)	Pu (Bq/kg)	u (Bq/kg)	C ^{137}Cs (Bq/kg)	u (Bq/kg)	ti.y	uti.y	Ti (A.D.)	^{210}Pb (Bq/kg)	u.Bq/kg
0.5	MDC		973	41	0.7	0.1	2020.3	124	18
1.5	MDC		1195	82	1.8	0.2	2019.2	172	19
2.5	MDC		1305	87	2.5	0.2	2018.5	179	19
3.5	MDC		1054	67	3.2	0.3	2017.8	138	21
4.5	MDC		811	39	4.1	0.4	2016.9	128	13
5.5	MDC		701	25	5.3	0.5	2015.7	176	9
6.5	MDC		615	81	6.1	0.5	2014.9	322	46
7.5	MDC		454	21	6.9	0.6	2014.1	196	17
8.5	MDC		499	14	8.5	0.8	2012.5	204	10
9.5	MDC		382	19	10.1	0.9	2010.9	335	24
10.5	MDC		367	32	11.8	1.1	2009.2	347	23
11.5	MDC		471	26	13.7	1.2	2007.3	494	22
12.5	MDC		513	19	15.5	1.4	2005.5	618	26
13.5	MDC		542	20	17.5	1.6	2003.5	531	26
14.5	MDC		356	15	19.6	1.8	2001.4	388	20
15.5	MDC		512	14	21.5	1.9	1999.5	272	8
16.5	MDC		483	19	23.2	2.1	1997.8	172	16
17.5	0.74	0.08	659	16	25.1	2.2	1995.9	168	8
18.5	0.19	0.03	2334	97	26.7	2.4	1994.3	351	31
19.5	0.04	0.00	2576	55	28.4	2.5	1992.6	192	7
20.5	0.05	0.01	511	12	30.5	2.7	1990.5	118	5
21.5	0.10	0.01	454	9	33.1	3.0	1987.9	112	7
22.5	0.04	0.00	501	15	35.9	3.2	1985.1	115	11
23.5	0.18	0.01	686	28	37.8	3.4	1983.2	195	16
24.5	0.44	0.06	408	12	39.6	3.5	1981.4	134	10
25.5	0.67	0.07	336	10	42.0	3.8	1979.0	147	8
26.5	0.94	0.10	342	15	44.3	4.0	1976.7	149	13
27.5	4.91	0.34	549	15	46.6	4.2	1974.4	173	8
28.5	10.70	0.69	512	8	49.8	4.5	1971.2	128	5
29.5	20.90	3.79	439	12	53.0	4.7	1968.0	89	6
30.5	24.12	1.57	394	11	55.3	4.9	1965.7	69	5
31.5	17.99	1.18	308	10	57.4	5.1	1963.6	62	5
32.5	11.64	0.82	310	7	59.6	5.3	1961.4	53	3
33.5	5.72	0.39	164	7	61.7	5.5	1959.3	46	5
34.5	5.86	0.50	139	6	63.6	5.7	1957.4	69	8
35.5	3.32	0.30	117	4	65.6	5.9	1955.4	49	3
36.5	1.84	0.16	145	3	67.8	6.1	1953.2	36	2
37.5	1.64	0.17	136	8	69.5	6.2	1951.5	41	5
38.5	0.91	0.13	116	6	70.7	6.3	1950.3	42	5
39.5	1.11	0.15	79	4	72.1	6.5	1948.9	32	6
40.5	0.41	0.06	95	7	74.0	6.6	1947.0	35	7

Supplementary table 2 presents results of $F^{14}C$ measurements and age depth modelling of analysed macrofossils of Sn0.
***Polytrichium strictum* stems with leaves. *Sphagnum* stems were selected except for sample Sn049-50. where *Sphagnum russowi* stem s was provided.**

Sample Code	ETH-	C14 age BP	±1ó	F14C	±1ó	äC13 ‰	±1ó	mg C	C/N at	%C	Method1	Modelled (BCE/CE) from	to
Sn049-50	ETH-125880	136	22	**0.9830**	0.0026	-2.4	1.0	0.95	157.0599	41.496	ABA 60°	**1900**	**1943**
Sn044.5	ETH-125881	134	22	**0.9830**	0.0027	-2.6	1.0	0.95	104.3285	44.2674	ABA 60°	**1911**	**1944**
Sn040-41	ETH-125882	174	22	**0.9790**	0.0026	-2.5	1.0	0.95	86.8694	43.641	ABA 60°	**1920**	**1946**
Sn039.5	ETH-125883	121	22	**0.9850**	0.0027	-2.7	1.0	0.95	133.9193	41.7051	ABA 60°	**1925**	**1948**
Sn037.5	ETH-125884	-893	21	**1.1180**	0.0030	-2.7	1.0	0.95	116.8599	44.1514	ABA 60°	**outlier**	**outlier**
Sn035.5	ETH-125885	222	22	**0.9730**	0.0026	-2.5	1.0	0.95	126.0526	41.0112	ABA 60°	**1939**	**1952**
Sn033.5	ETH-125886	213	22	**0.9740**	0.0026	-2.6	1.0	0.95	94.22811	45.3861	ABA 60°	**1944**	**1953**
Sn031.5	ETH-125887	-463	21	**1.0590**	0.0028	-2.5	1.0	0.95	122.7853	41.8927	ABA 60°	**1956**	**1957**
Sn030-31	ETH-125888	-1434	21	**1.1950**	0.0032	-2.6	1.0	0.95	110.9643	42.3224	ABA 60°	**1958**	**1961**
Sn028.5	ETH-125889	-3528	21	**1.5510**	0.0040	-2.7	1.0	0.95	122.3474	47.6966	ABA 60°	**1969**	**1971**
Sn026.5	ETH-125890	-2071	21	**1.2940**	0.0034	-2.7	1.0	0.95	82.97971	42.2417	ABA 60°	**1979**	**1980**
Sn024-25	ETH-125891	-1244	21	**1.1670**	0.0031	-2.7	1.0	0.95	97.4935	44.6352	ABA 60°	**1988**	**1990**
Sn022.5	ETH-125892	-1020	21	**1.1350**	0.0030	-2.8	1.0	0.95	107.9701	39.8283	ABA 60°	**1991**	**1993**
Sn020.5	ETH-125893	-810	21	**1.1060**	0.0029	-2.6	1.0	0.95	106.5836	42.6141	ABA 60°	**1996**	**1999**